TOPICAL REVIEW • OPEN ACCESS

Probing beyond the standard model physics with double-beta decays

To cite this article: Elisabetta Bossio and Matteo Agostini 2024 *J. Phys. G: Nucl. Part. Phys.* **51** 023001

View the article online for updates and enhancements.

Topical Review

Probing beyond the standard model physics with double-beta decays

Elisabetta Bossio[1,2,*] and Matteo Agostini[3]

[1] Physik Department, Technische Universität München, Germany
[2] IRFU, CEA, Université Paris-Saclay, France
[3] Department of Physics and Astronomy, University College London, London, United Kingdom

E-mail: Elisabetta.bossio@cea.fr and matteo.agostini@ucl.ac.uk

Abstract

Nuclear double-beta decays are a unique probe to search for new physics beyond the standard model. Hypothesized particles, non-standard interactions, or the violation of fundamental symmetries would affect the decay kinematics, creating detectable and characteristic experimental signatures. In particular, the energy distribution of the electrons emitted in the decay gives an insight into the decay mechanism and has been studied in several isotopes and experiments. No deviations from the prediction of the standard model have been reported yet. However, several new experiments are underway or in preparation and will soon increase the sensitivity of these beyond-the-standard-model physics searches, exploring uncharted parts of the parameter space. This review brings together phenomenological and experimental aspects related to new-physics searches in double-beta decay experiments, focusing on the testable models, the most-sensitive detection techniques, and the discovery opportunities of this field.

Keywords: double-beta decay, neutrino properties, particle physics, beyond the standard model physics

* Author to whom any correspondence should be addressed.

1. Introduction

Double-β decays are nuclear transitions in which an isotope changes its atomic number Z by two units, while maintaining a constant mass number A:

$$(A, Z) \rightarrow (A, Z + 2) + ... \tag{1}$$

This process can occur only if the conversion of two protons into two neutrons leads to a more bounded nuclear configuration, with a positive Q-value defined as $Q_{\beta\beta} \approx M(A, Z)c^2 - M(A, Z + 2)c^2$ [1], where M refers to the mass of the neutral isotopes. Different theory models predict different decay final states. However, in general, they all envision the production of two electrons to conserve the electric charge, along with neutral particles.

These decays are a second-order weak process. Thus, they can be observed only in isotopes for which the otherwise dominant first-order transitions—and in particular, the single-β decay—are strongly suppressed. This is the case for a limited number of even–even nuclei for which the single-β decay is energetically forbidden, as the attractive nuclear pairing interaction makes them more bound than their odd–odd neighbors but less than their even–even second-neighbors (see figure 1). Alternatively, candidate isotopes for the observation of double-β transitions are also those for which the single-β decay is suppressed by the large mismatch between the total angular momentum of the initial and final nuclei [2].

Double-β decays were postulated in 1935 [3] by Maria Goeppert-Maier, who pointed out how these transitions could proceed through the 'simultaneous emission of two electrons and two (anti)neutrinos':

$$(A, Z) \rightarrow (A, Z + 2) + 2e^- + 2\overline{\nu} \tag{2}$$

In this case, the decay would 'appear as the simultaneous occurrence of two transitions, each of which does not fulfill the law of conservation of energy separately'. This final state is the only one allowed by the standard model (SM) of particle physics and is typically referred to as 'two-neutrino double-β' ($2\nu\beta\beta$) decay (figure 2, Left).

The discovery of double-β transitions traces back to the observation of the decay daughter isotope (^{130}Xe) in a geochemical experiment[4] with ^{130}Te [4]. Only 40 years later, double-β decays were observed in real-time through a calorimetric measurement of the energy released by the electron emitted in the decay of ^{82}Se into ^{82}Kr [5]. The electron summed energy distribution was found to have a continuous shape compatible with the expectations for Goeppert-Maier's $2\nu\beta\beta$ decay (figure 3). To date, double-β transitions compatible with the $2\nu\beta\beta$ final state have been observed in nine isotopes with half-life values in the range of 10^{18}–10^{24} years [6], making it one of the rarest processes ever measured.

Theories beyond the standard model (BSM) predict a variety of new, additional final states involving the emission of electrically neutral exotic particles, which would affect the decay kinematics and alter the energy and angular distributions of the electrons emitted in the decay. Similarly, the violation of fundamental symmetries would affect the decay kinematics. However, despite many past and recent experiments, no deviations from the SM's $2\nu\beta\beta$-decay expectations have yet been observed. In some cases, double-β decay experiments set bounds on new physics parameters that cannot be accessed by any other direct search, offering a unique window to the underlying BSM theories. In other cases, bounds obtained with double-β decay experiments are (or will be in future experiments) covering previously unexplored regions of the parameter spaces, offering a complementary probe of the relevant BSM theories.

---

[4] The geochemical method is based on extracting and counting the number of daughter atoms of double-β transitions accumulated over long geological times in an ancient mineral containing the parent double-β decay isotope.
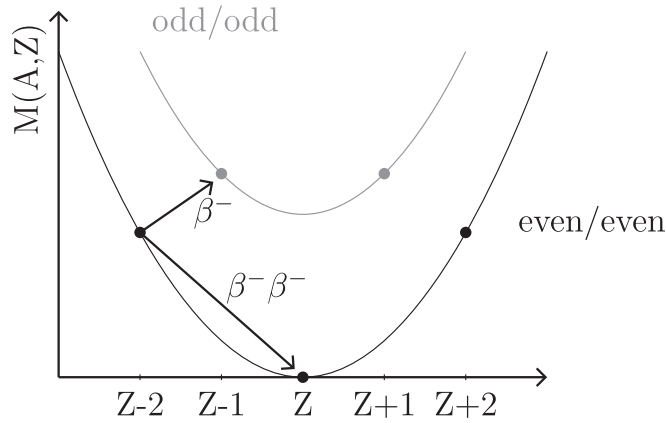
Figure 1. Mass parabola of nuclear isobars with even mass number A. Due to the pairing term in the semi-empirical mass formula, β^- transitions of even/even nuclei to their odd/odd isobaric neighbor can be energetically forbidden, whereas, in a second-order process, $\beta^-\beta^-$ decay is allowed.
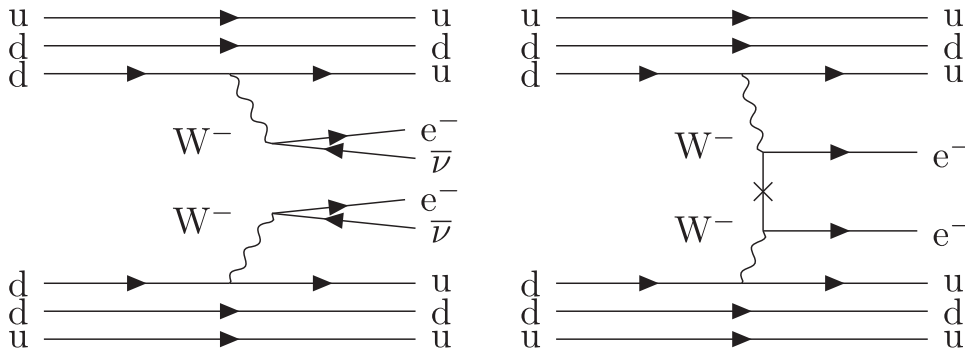

Figure 2. (Left) Feynman diagram of the SM $2\nu\beta\beta$ decay. (Right) Feynman diagram of the lepton number non-conserving $0\nu\beta\beta$ decay in the light-neutrino exchange scenario.

Double-β decay searches have been historically carried out in experiments primarily built to study a hypothesized final state with only two electrons, i.e. without neutrinos (figure 2, Right), in which the summed electron energy is expected to be precisely equal to $Q_{\beta\beta}$ rather than a continuous distribution (figure 3). Such 'neutrinoless double-β' ($0\nu\beta\beta$) decay is indeed predicted by leading theories explaining the matter-antimatter asymmetry in our Universe and the origin of neutrino masses. Its search has been an indisputable priority of the particle physics community for the last two decades. Currently, ton-scale double-β-decay experiments are under preparation with the ultimate goal of increasing the sensitivity to $0\nu\beta\beta$-decay half-life values by two orders of magnitudes compared to current constraints, up to 10^{28} years. We refer the reader to [7] for a recent review on $0\nu\beta\beta$ decay.

Thanks to their planned ultra-low background level and huge target mass, the next generation of double-β decay experiments will provide high-precision measurements of the $2\nu\beta\beta$-decay, enabling new opportunities to discover new final states. This motivates the timing of our work. Indeed, although several review articles have discussed double-β decay searches in recent years, they have typically focused on the $2\nu\beta\beta$-decay final state. For
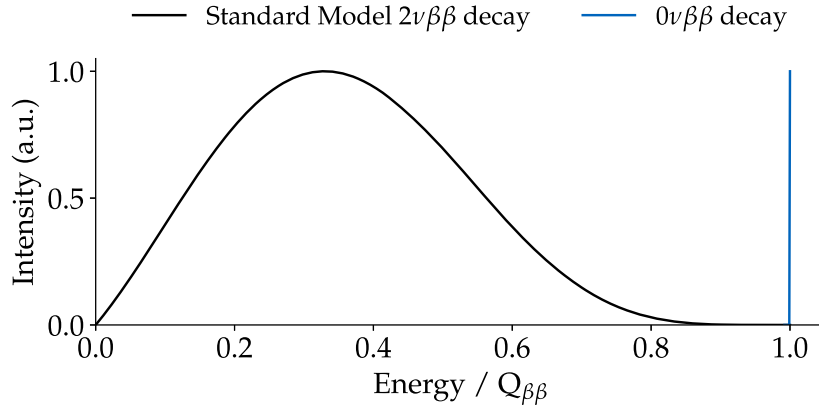
Figure 3. Summed electron energy distribution for the SM $2\nu\beta\beta$ decay and the lepton number non-conserving $0\nu\beta\beta$ decay. An infinite energy resolution is assumed, and an arbitrary normalization is used for illustrative purposes.

instance, we would like to highlight [8] that gives an excellent review of $2\nu\beta\beta$-decay's history and [9] for a recent summary of the field. Our review is the first that focuses on BSM searches, covering their theoretical and experimental aspects, current constraints, and ongoing endeavor to improve the experimental sensitivities. Future $0\nu\beta\beta$ decay experiments with leading sensitivity will measure only the summed energy of the two final state electrons—aiming to distinguish the $0\nu\beta\beta$ decay peak at $Q_{\beta\beta}$ from the continuous $2\nu\beta\beta$ decay distribution—without having access to the single electron energy or electron angular correlation. Thus, this review focuses on how BSM physics would affect the summed electron energy distribution and how this can be exploited to search for BSM double-β decays.

The manuscript is organized as follows. We first briefly discuss the SM $2\nu\beta\beta$ decay in section 2 for completeness. We then review in section 3 the phenomenology of double-β transitions mediated by BSM processes. Section 4 is dedicated to the experimental signatures that experiments can exploit. It also contains an original contribution to the field, which is the first derivation of analytical formulae describing the experimental sensitivity as a function of key experimental parameters and systematic uncertainties. We finally summarize, in section 5, the latest experimental results and, in section 6, highlight the role of future double-β decay experiments in exploring the parameter spaces and relate these constraints to other probes if they exist.

2. Standard model allowed double-β decay

Double-β transitions can be uniquely identified by the production of the daughter nucleus. With this principle, the double-β decay of ^{130}Te was first detected in 1950 with a geochemical experiment. The detection of an excess of ^{130}Xe was proof of the double-β decay of the initial nucleus and allowed a first determination of its half-life [4]. Even if this result was initially not considered seriously, it represents the first observation of $2\nu\beta\beta$ decay, as became clear over the next fifteen to twenty years.

In fact, after both the $2\nu\beta\beta$ and $0\nu\beta\beta$ decays were proposed (1935–1939), the first estimate of the half-life of the two processes strongly favored the $0\nu\beta\beta$ decay. This was predicted with a half-life of the order of 10^{15} years, whereas a half-life of about 10^{21} years was predicted for the SM allowed $2\nu\beta\beta$ decay. Only the discovery of parity violation in 1957 and the

determination of the V–A nature of weak interactions made clear that the probability of $0\nu\beta\beta$ decay had to be much smaller than that of $2\nu\beta\beta$ decay.

In the following years, new geochemical experiments were performed, confirming the observation of the $2\nu\beta\beta$ decay of ^{130}Te [10, 11] and observing for the first time the $2\nu\beta\beta$ decay of ^{82}Se [11] and ^{128}Te [12].

A key milestone in the history of double-β decays occurred in 1985 when Doi, Kotani and Takasugi first computed the energy and angular distributions of the electrons emitted in double-β decays, providing a clear signature to distinguish the SM allowed $2\nu\beta\beta$ decay from BSM double-β decays [13]. In the same work, figure 3 appeared for the first time.

Following these theory developments, the first direct observation of a $2\nu\beta\beta$ decay was made in 1987 using a ^{82}Se time projection chamber, which could measure the summed energy distribution of the two electrons and extract the ^{82}Se $2\nu\beta\beta$-decay half-life based on 36 observed events. This was a turning point in the history of $2\nu\beta\beta$ decays, and in the following ten years $2\nu\beta\beta$ decay was directly observed in seven isotopes: ^{76}Ge [14], ^{100}Mo [15–18], ^{82}Se [19, 20], ^{116}Cd [21–24], ^{48}Ca [25], ^{150}Nd [17], ^{96}Zr [26]. In addition to the summed electrons' energy distribution, which was measured for all the above-mentioned isotopes, the NEMO-2 experiment also measured the single electron energy and the angular distributions of the electrons for ^{100}Mo, ^{116}Cd, ^{82}Se, and ^{96}Zr [18, 20, 22, 24, 26]. In the same years, the $2\nu\beta\beta$ decay of ^{238}U was first observed in a radiochemical experiment [27].

By the end of the 20th century, the energy and half-life of $2\nu\beta\beta$ decay had been measured for 10 isotopes in direct, geochemical, and radiochemical experiments. In addition, in the last two decades, direct observations of the $2\nu\beta\beta$ decay of ^{130}Te and ^{136}Xe were reported in 2010 [28] and 2011 [29], respectively. Table 1 summarises the double-β decaying isotopes for which the $2\nu\beta\beta$ decay has been directly observed so far.

The precision with which experiments were able to determine the half-life of $2\nu\beta\beta$ decays has increased over the years, with modern experiments reaching a percent-level precision for most of the isotopes. The most precise measurements of the $2\nu\beta\beta$ decay half-life are summarised in table 1.

In addition to the Goeppert-Maier's $2\nu\beta\beta$ decay (equation (2)) or $\beta^-\beta^-$ transition, three additional second-order transitions can be allowed in the SM depending on the relative numbers of protons and neutrons in the nucleus:

$$(\beta^+\beta^+):\ (A,\,Z) \rightarrow (A,\,Z-2) + 2e^+ + 2\nu \tag{3a}$$

$$(ECEC):\ (A,\,Z) + 2e^- \rightarrow (A,\,Z-2) + 2\nu \tag{3b}$$

$$(EC\beta^+):\ (A,\,Z) + e^- \rightarrow (A,\,Z-2) + e^+ + 2\nu. \tag{3c}$$

The energy released in the three processes listed above is smaller than the $\beta^-\beta^-$ decay in equation (2) because it is reduced by the electron mass and/or by the binding energy of the captured electrons. Consequently, these processes have lower probabilities than the $\beta^-\beta^-$ decay owing to the smaller phase space, and even when they exhibit clear experimental signatures, the longer half-life values pose a limit to their experimental observation. In the following, we will always refer to the $\beta^-\beta^-$ process as double-β decay.

In nature, there are 35 isotopes that can undergo $2\nu\beta\beta$ decay, and 34 more that can undergo $\beta^+\beta^+$, $ECEC$, and $EC\beta^+$ [40]. In fact, not all of them fulfill the experimental requirements, e.g., high isotopic abundance, large $Q_{\beta\beta}$ value, and compatibility with experimental technologies. To date, only the nine isotopes listed in table 1 have been used in direct search experiments.

The rate of $2\nu\beta\beta$ decay can be calculated following Fermi's golden rule for β decay. To a good approximation, the kinematic part (the phase space of the leptons emitted in the decay)

Table 1. Direct observations of $2\nu\beta\beta$ decays. The year of the first observation is indicated for each isotope, together with the most precise half-life determination. The uncertainty shown is the sum in quadrature of the statistical and systematic uncertainties, when available.

Isotope	First observation	Half-life	Experiment
$^{48}\text{Ca} \to {}^{48}\text{Ti}$	1996 [25]	$(6.4^{+1.4}_{-1.1}) \times 10^{19}$	NEMO-3 [30]
$^{76}\text{Ge} \to {}^{76}\text{Se}$	1990 [14]	$(2.022 \pm 0.041) \times 10^{21}$	GERDA [31, 32]
$^{82}\text{Se} \to {}^{82}\text{Kr}$	1987 [5]	$(8.60^{+0.19}_{-0.13}) \times 10^{19}$	CUPID-0 [33]
$^{96}\text{Zr} \to {}^{96}\text{Mo}$	1999 [26]	$(2.35 \pm 0.21) \times 10^{19}$	NEMO-3 [34]
$^{100}\text{Mo} \to {}^{100}\text{Ru}$	1991 [15, 16]	$(7.12^{+0.21}_{-0.17}) \times 10^{18}$	CUPID-Mo [35]
$^{116}\text{Cd} \to {}^{116}\text{Sn}$	1995 [21–23]	$(2.63^{+0.11}_{-0.12}) \times 10^{19}$	Aurora [36]
$^{130}\text{Te} \to {}^{130}\text{Xe}$	2010 [28]	$(7.71^{+0.14}_{-0.16}) \times 10^{20}$	CUORE [37]
$^{136}\text{Xe} \to {}^{136}\text{Ba}$	2011 [29]	$(2.165 \pm 0.063) \times 10^{21}$	EXO-200 [38]
$^{150}\text{Nd} \to {}^{150}\text{Sm}$	1997 [17]	$(9.34^{+0.66}_{-0.64}) \times 10^{18}$	NEMO-3 [39]

and the nuclear part (the matrix element responsible for the transition probability between the two nuclear states) can be factorized as:

$$\Gamma^{2\nu} = [T^{2\nu}_{1/2}]^{-1} = |\mathcal{M}^{2\nu}|^2 \, \mathcal{G}^{2\nu}(Q_{\beta\beta}, Z), \tag{4}$$

where $\mathcal{G}^{2\nu}$ is the phase-space factor and is obtained by integrating over the phase space of the four leptons, and $\mathcal{M}^{2\nu}$ is the nuclear matrix element (NME) and deals with the nuclear structure of the transition. While the phase-space factor can be calculated exactly, the NME is much more difficult to evaluate and relies on nuclear structure models.

Methods for the phase-space factor calculation for the $2\nu\beta\beta$ decay have been developed in several works [13, 41–44]. We report the expression of the phase space following [44]:

$$\mathcal{G}^{2\nu} = \frac{2\tilde{A}^2}{3\ln 2} \frac{(G_F \cos\theta_C)^4}{64\pi^2} \int_{m_e}^{Q_{\beta\beta}+m_e} \int_{m_e}^{Q_{\beta\beta}+m_e-E_{e1}} \int_0^{Q_{\beta\beta}-E_{e1}-E_{e2}} f_{11}^{(0)}$$
$$\times (\langle K_N \rangle^2 + \langle L_N \rangle^2 + \langle K_N \rangle \langle L_N \rangle) \, p_{\nu_1}^2 p_{\nu_2}^2 p_1 E_1 p_2 E_2 \, \mathrm{d}p_{\nu_1} \mathrm{d}E_{e1} \mathrm{d}E_{e2}. \tag{5}$$

The strength of the interaction is given by $(G_F \cos\theta_C)^4$, with the Fermi constant $G_F = 1.16 \times 10^{-5} \, \text{GeV}^{-2}$ and the Cabibbo angle θ_C. The quantity $\tilde{A}$ denotes the excitation energy with respect to the average of the initial and final ground states and can be written as a function of the $Q_{\beta\beta}$, a suitable chosen excitation energy of the intermediate nucleus $\langle E_N \rangle$, and the energy of the initial nucleus E_I:

$$\tilde{A} = \frac{1}{2}(Q_{\beta\beta} + 2m_e) + \langle E_N \rangle - E_I. \tag{6}$$

The notation $\langle K_N \rangle$ and $\langle L_N \rangle$ stay for:

$$\langle K_N \rangle = \frac{1}{E_{e1} + p_{\nu_1} + \langle E_N \rangle - E_I} + \frac{1}{E_{e2} + p_{\nu_2} + \langle E_N \rangle - E_I}, \tag{7}$$

$$\langle L_N \rangle = \frac{1}{E_{e1} + p_{\nu_2} + \langle E_N \rangle - E_I} + \frac{1}{E_{e2} + p_{\nu_1} + \langle E_N \rangle - E_I}. \tag{8}$$

The energy and momentum of the two outgoing electrons are denoted by E_{e1}, E_{e2}, p_{e1}, and p_{e2}, while p_{ν_1} and p_{ν_2} are the momentum of the emitted neutrinos, with the latter fixed by

energy conservation $p_{\nu_2} = Q_{\beta\beta} - E_{e1} - E_{e2} - p_{\nu_1}$. Finally, the factor $f_{11}^{(0)}$ originates from the Coulomb interaction of the electrons with the daughter nucleus.

We note that we have used, in all previous equations and will use in the rest of the review, the natural units $\hbar = c = 1$ so that, for example, masses are expressed in eV.

From the phase space in equation (5), the distribution of the summed kinetic energy of the two electrons $K = E_{e1} + E_{e2} - 2m_e$ can be obtained:

$$\frac{\mathrm{d}\Gamma^{2\nu}}{\mathrm{d}K} = |\mathcal{M}^{2\nu}|^2 \, \frac{\mathrm{d}\mathcal{G}^{2\nu}}{\mathrm{d}K}. \tag{9}$$

To a first approximation, the shape of this distribution is determined only by the phase space. The contribution of the NME to it is small and primarily affects the absolute value of the transition probability.

The summed energy of the two electrons emitted in the $2\nu\beta\beta$ decay is continuously distributed between 0 and the endpoint at the $Q_{\beta\beta}$ value due to the neutrinos escaping the detector and carrying away part of the energy.[5] This is shown in figure 3, compared to the $0\nu\beta\beta$ decay, for which a δ function at $Q_{\beta\beta}$ is expected because all the transition energy goes into the kinetic energy of the two electrons.

In conclusion, we have seen that although the first observation of $2\nu\beta\beta$ decay is commonly traced back to 1950 and the first geochemical experiment with ^{130}Te, it took many years for the community to acknowledge that the production of the daughter nucleus observed in this first experiment was exactly the result of Goeppert-Maier's $2\nu\beta\beta$ decay. To date, precision measurements of the $2\nu\beta\beta$ decay of several isotopes and the agreement between the distribution of multiple observables (summed electron energies, single electron energy, and angular distributions) with their theoretical prediction are striking evidence for the $2\nu\beta\beta$ decay and exclude a large part of the parameter space for many BSM theories.

3. Beyond-standard-model physics in double-β decay

If new particles were involved in a double-β decay, or any new physics affected the phase space of the two electrons emitted in the $2\nu\beta\beta$ decay, then the summed electron energy distribution predicted by BSM theory would differ from that predicted for the SM $2\nu\beta\beta$ decay (equation (9), figure 3). This is the main feature used to search for these BSM decays in the experimental data. Single-electron energy distributions and electron angular distributions are also primarily determined by the phase space, and are characteristic of the physics model and decay final state. Experiments that can also measure these distributions can strongly enhance their sensitivity in distinguishing the SM allowed $2\nu\beta\beta$ decay from BSM double-β decays. In this review, we focus on BSM sensitivity using the first observable. This is because the calorimetric measurement approach pursued in the next generation of $0\nu\beta\beta$ decay experiments with leading sensitivities gives access only to the summed electron energy distribution.

We classify the BSM models into three groups. The first one contains those predicting the existence of new particles—either bosons or fermions—which are emitted in the decay, replacing one or both of the $2\nu\beta\beta$'s neutrinos. The second one includes theories in which fundamental symmetries such as Lorentz covariance or Pauli's exclusion principle are violated. The last group covers non-standard interactions, like right-handed leptonic currents and strong neutrino self-interactions.

---

[5] To be precise, the maximum energy is $Q_{\beta\beta}$ minus the mass of the two emitted neutrinos. This is typically neglected as Q-values are at the MeV-energy scale, while neutrino masses are smaller than the eV-energy scale [45, 46].

3.1. New particles

3.1.1. Bosons.   In the early 1980s, an attractive approach to the neutrino mass problem was considered in which the neutrinos are Majorana particles with small masses arising from the spontaneous breakdown of the global *B–L* symmetry, where *B* is the baryon number and *L* is the lepton number. In these models, a massless Goldstone boson should exist, which was called the 'Majoron'. Several realizations of this idea were proposed, mainly differing by the weak isospin (*I*) properties of the Majoron and leading to different phenomenology.

The first model was proposed by Chikashige, Mohapatra, and Peccei [47, 48]. In this model, the Majoron arises from a Higgs singlet ($I = 0$) and gives rise to small neutrino masses via the 'see-saw' mechanism. However, the Majoron coupling to neutrino is so small that it would be very hard to test it through laboratory experiments. Shortly after, Gelmini and Roncadelli proposed a model in which the Majoron arises from a Higgs triplet ($I = 1$) [49]. In this second case, a stronger coupling to neutrinos would be possible. A third case was considered later in 1987, in relation to solar neutrino oscillations, where the Majoron arises from a Higgs doublet ($I = 1/2$), possibly leading to strong coupling to neutrinos [50–52].

If the Majoron Yukawa coupling to neutrinos were sufficiently strong ($\sim 10^{-5}$–10^{-3}), this would have interesting consequences for particle physics, astrophysics, and cosmology. By 1981, starting from the Gelmini-Roncadelli Majoron model, a rich phenomenology was derived [53]. One of the most interesting consequences considered at that time was the possibility of emitting such a Majoron in double-β decays, giving rise to a new final state in which two electrons and a Majoron (and no neutrinos) are present (figure 4, Left). The decay rate of this process was calculated, and constraints on the neutrino-Majoron coupling were set using existing limits on the decay rate of $0\nu\beta\beta$ decay [54]. In fact, at that time, the possibility of distinguishing $2\nu\beta\beta$, $0\nu\beta\beta$, or double-β decay with the emission of a Majoron was not conceived, and the latter was regarded only as 'an interesting possibility, which may confuse the analysis of double-β decay experiments' [55]. Only the impressive theoretical work of Doi, Kotani, and Takasugi, in which the energy and angular distribution of the electrons emitted in the double-β decay with the emission of a Majoron were calculated for the first time [13], provided a clear experimental signature to distinguishing different double-β decay channels. The same authors revised and updated these calculations in a successive work [56]. In the same time period, a supersymmetric model was developed, which would lead to the emission of two Majorons in double-β decays [57].

It was clear that the Majoron with nontrivial weak isospin properties (such as the triplet and doublet Majoron), which would have appreciable coupling to neutrinos, would also have a strong coupling to the other leptons and would necessarily be discovered in the upcoming electron-positron colliders [54]. The LEP limits on the number of active light-neutrino species ruled out both triplet and doublet Majoron models [58, 59]. At the same time, the first direct double-β decay experiments started to search for double-β decay with Majoron emission, and an excess of events below $Q_{\beta\beta}$ was observed, which could be compatible with the energy distribution predicted by Doi *et al* for such decays [60–62]. However, the singlet Majoron model, the only available model aligning with LEP data, faced limitations. In its original Chikashige-Mohapatra-Peccei formulation, the Majoron exhibited such weak coupling to neutrinos that the half-life of the resulting double-β decay far exceeded the sensitivity of the experiments, which was on the order of 10^{20}–10^{21} years.

These events motivated a number of models able to reconcile the results on the *Z* decay width with a neutrino-Majoron coupling strong enough to explain the event excess: new models with a singlet Majoron [63], models in which the Majoron carries a non-zero lepton number [64, 65], models predicting the emission of two Majorons [66], and models in which,
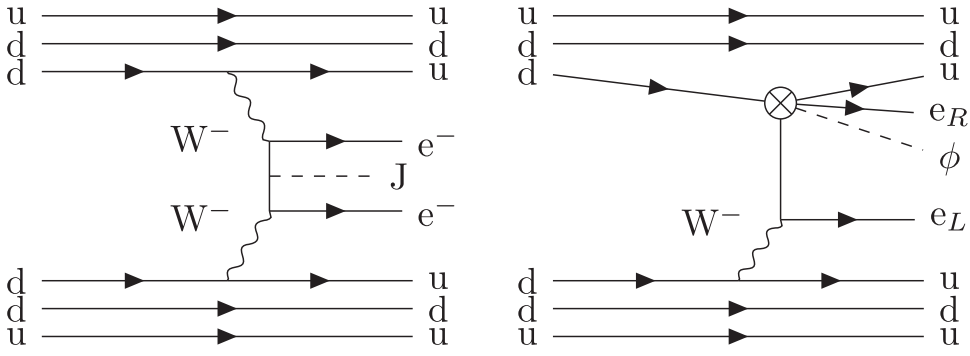
Figure 4. (Left) Feynman diagram for the double-β decay with the emission of a Majoron in classical models. (Right) Feynman diagram for the emission of a Majoron-like particle ϕ through an effective dimension-seven operator containing right-handed currents in double-β decay Reproduced from [53]. CC BY 4.0.

departing from the original conception of the Majoron as Goldstone boson, the Majoron arises as the component of a massive gauge boson [67] or a bulk field [68].

This ensemble of models can lead to two different final states, corresponding to the emission of one or two Majorons, which we will indicate with J:

$$(A, Z) \rightarrow (A, Z + 2) + 2e^- + J, \tag{10a}$$

$$(A, Z) \rightarrow (A, Z + 2) + 2e^- + 2J. \tag{10b}$$

The rate of the double-β decay with the emission of one or two Majorons can be expressed as:

$$\Gamma^J = g_{J\alpha}^2 \, |\mathcal{M}_\alpha^J|^2 \, \mathcal{G}_\alpha^J, \tag{11a}$$

$$\Gamma^{JJ} = g_{J\alpha}^4 \, |\mathcal{M}_\alpha^{JJ}|^2 \, \mathcal{G}_\alpha^{JJ}, \tag{11b}$$

where $g_{J\alpha}$ is the neutrino-Majoron coupling, $\mathcal{M}_\alpha^{J(JJ)}$ the NME, and $\mathcal{G}_\alpha^{J(JJ)}$ the phase-space factor. All three terms depend on the particular model, which we indicated with the subscript α. Systematic calculations of phase-space factors and NMEs for a number of Majoron models were performed in [69] for many isotopes. More recently, improved calculations of the summed electron energy distributions have been performed, leading to improved calculations of the phase-space factors [70]. These calculations align with the state-of-the-art in the field, employing exact Dirac wave functions with finite nuclear size and electron screening, adhering to the approach employed for the SM $2\nu\beta\beta$ decay and $0\nu\beta\beta$ decay calculations [44]. Improved calculations of the NMEs have also been performed with more modern tools [71]. We will discuss the NMEs in the context of BSM physics searches with double-β decays in section 4.5.

If one or two Majorons are emitted in the double-β decay, they would escape any detector and carry away part of the decay energy. In analogy with the $2\nu\beta\beta$ decay, the summed electron energy is continuously distributed between 0 and $Q_{\beta\beta}$, and its exact shape is primarily determined by the phase space. In turn, the phase space depends on the Majoron model, particularly on the effective neutrino-Majoron interaction Lagrangian leading to the Majoron-emitting double-β decay. This can be parameterized to a first approximation with a spectral index n:
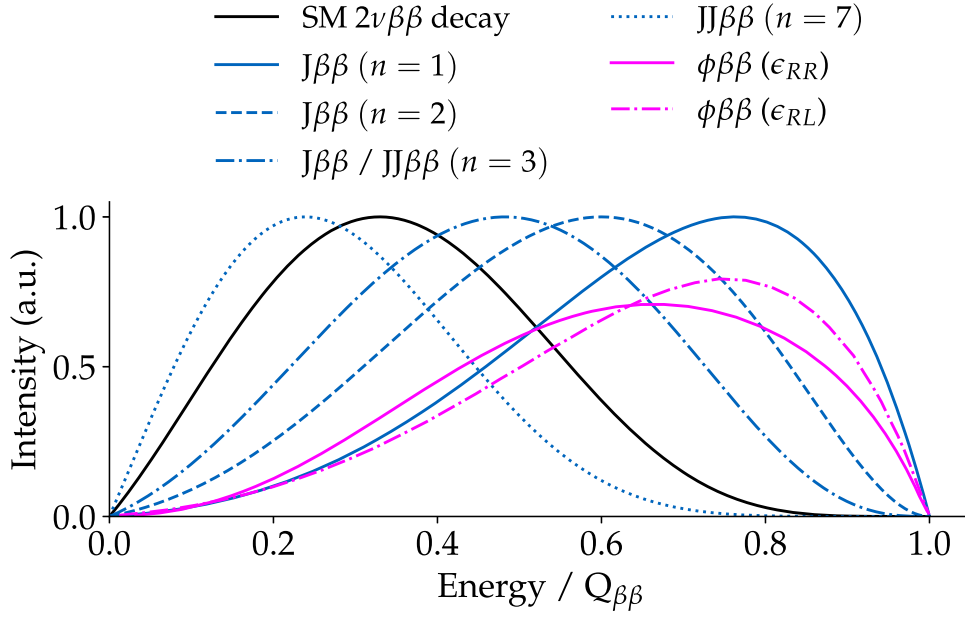
Figure 5. Summed electron energy distribution for different Majoron models (the spectral index corresponding to each model is indicated) compared to the SM $2\nu\beta\beta$ decay distribution for the ^{76}Ge isotope. The decays with the emission of a non-standard Majoron are also shown: they can be triggered by an effective seven-dimension operator, containing right-handed (ϵ_{RR}^{ϕ}) and left-handed (ϵ_{RL}^{ϕ}) hadronic current. The latter two were adapted from [53]. An infinite energy resolution is assumed, and an arbitrary normalization is used for illustrative purposes. Reproduced from [53]. CC BY 4.0.

$$\frac{\mathrm{d}\Gamma^J}{\mathrm{d}K} \propto \frac{\mathrm{d}\mathcal{G}^J}{\mathrm{d}K} \sim (Q_{\beta\beta} - K)^n. \tag{12}$$

Figure 5 shows the summed electron energy distribution for different Majoron models compared to the SM $2\nu\beta\beta$ decay distribution.

The spectral index is commonly used to group models predicting the same experimental signature, i.e. the same summed electron energy distribution. These models are not distinguishable by the experiments. Table 2 shows a summary of all the Majoron models grouped by the number of emitted Majorons in the second column, the spectral index in the third column, and the Majoron's properties in the last two columns. The fourth column indicates whether the Majoron is a Goldstone boson or not, whereas the last column shows the Majoron's leptonic charge. Models in which the Majoron carries a lepton number different from 0 preserve the lepton number symmetry. Without an independent test of lepton number violation, these models are experimentally indistinguishable from the corresponding lepton number non-conserving processes.

All the models discussed so far focus on the emission of one or two Majorons originating from the intermediate neutrino exchanged in the process. Despite the differences among the models, i.e. the different effective neutrino-Majoron interaction Lagrangians, all of them assume the SM V–A structure of the charged currents involving leptons and quarks. We will refer to them as 'classical' models. Recently a new scenario has been considered, in which a

Majoron-like particle (ϕ) is emitted in the double-β decay ($\phi\beta\beta$ decay). In this case, the interaction is described by an effective dimension-seven operator, with right-handed lepton current and right/left-handed quark current [53]. The Feynman diagram of this process is shown in figure 4 together with the Majoron emission in classical models. The coupling strength between the neutrino and the Majoron-like ϕ is ϵ_{RL} if the effective operator contains left-handed quark currents, and ϵ_{RR} when the effective operator contains right-handed quark currents. The two cases have been considered separately, with only one of the two operators being present at a time.

The energy distribution predicted for the $\phi\beta\beta$ decay is also shown in figure 5. The distribution associated with ϵ_{RL} is very similar to the classical Majoron emission models leading to $n = 1$. On the other hand, introducing a hadronic right-handed current in the ϵ_{RR} term changes the shape of the distribution considerably.

In all the previous discussions, we assumed the Majoron to be massless. However, many of the models presented do not prevent the Majoron from being a light particle [53, 66, 72]. This possibility became extremely popular because light Majorons could be a dark matter candidate [73, 74]. If the Majoron mass is below the $Q_{\beta\beta}$, double-β decay with the emission of a Majoron can still happen. In this case, the endpoint of the energy distribution is shifted to $Q_{\beta\beta} - m_J$, where m_J is the Majoron mass.

3.1.2. Fermions. In many extensions of the SM, new spin $1/2$ particles, singlet under the SM gauge group, are introduced in relation to the question of neutrino mass generation or dark matter. Currently, the most popular exotic fermion is the sterile neutrino N. Sterile neutrinos are neutral and right-handed SM singlet fermions that interact with ordinary matter only through mixing with the active neutrinos. We refer the reader to [75] for a recent review of the theoretical and experimental motivation for sterile neutrinos, as well as their phenomenological consequence. In a variant of this scenario, the singlet fermion could be furnished with a Z_2 symmetry, so it can only be produced in pairs. In general, when a new exotic fermion is introduced in the theory, its mass and coupling to the SM particles are free parameters of the model. It is left to laboratory experiments and astrophysical and cosmological observations to probe the vast allowed parameter space.

In 1980, Shrock examined the possibility of searching for sterile neutrinos in β decays [76]. The admixture of one or more sterile neutrino states would create a discontinuity in the β decay spectrum similar to the discontinuity that a non-zero neutrino mass is expected to create at the endpoint. The position and amplitude of this kink would give information on the mass of the sterile neutrino and its mixing with the active neutrinos. Since then, several β decay experiments have searched for sterile neutrinos and have set the most stringent constraints in the mass range between $\sim$10 eV and $\sim$1 MeV [77–81].

In analogy with the case of single-β decays, sterile neutrinos with masses below few MeV could be produced in double-β decays. This possibility was recently discussed in [82, 83]. In [83], the production of exotic fermions in double-β decays was also extended to models in which single production is forbidden by additional symmetries while the pair production is allowed. Such a model could be realized with the neutral singlet fermion χ—a potential dark matter candidate—being charged under a discrete Z_2 symmetry to make it stable. This new fermion could interact with neutrinos through an effective four-fermion scalar interaction of the form $g_\chi \nu\nu\chi\chi$. This case is particularly interesting because such a particle cannot be produced in single-β decays, and double-β decays represent a unique discovery opportunity for laboratory experiments.

In general, models predicting the existence of light exotic fermions coupling with the SM neutrinos can lead to two additional double-β decay final states, corresponding to the

Table 2. Different Majoron models which predict double-β decays with the emission of one or two Majorons. The third column indicates the model's spectral index (n), the fourth column indicates whether the Majoron is a Goldstone boson or not, and the last column indicates the leptonic charge (L) of the Majoron. Models with a leptonic charge different from zero preserve the lepton number symmetry.

	Decay	n	Goldstone boson	L
a	J$\beta\beta$	1	yes	0
			no	0
			no	-2
b	J$\beta\beta$	2	Bulk field	0
c	J$\beta\beta$	3	yes	-2
			Gauge boson	-2
d	JJ$\beta\beta$	3	yes	0
			no	0
			no	-1
e	JJ$\beta\beta$	7	yes	-1

emission of one or two exotic fermions, which we will indicate with f:

$$(A, Z) \rightarrow (A, Z + 2) + 2e^- + \bar{\nu} + f, \tag{13a}$$

$$(A, Z) \rightarrow (A, Z + 2) + 2e^- + 2f. \tag{13b}$$

Sterile neutrinos can be produced via both (13a) and (13b) decay channels. Provided that both decay channels are kinematically allowed—i.e. the $Q_{\beta\beta}$ value must be larger than the sterile neutrino mass for the (13a) decay channel, and twice the sterile neutrino mass for the (13b) decay channel—the total double-β decay rate would become an incoherent sum of three channels:

$$\Gamma = \cos^4 \theta \, \Gamma_{\nu\nu} + 2 \cos^2 \theta \sin^2 \theta \, \Gamma_{\nu N} + \sin^4 \theta \, \Gamma_{NN}, \tag{14}$$

where $\sin^2 \theta$ represents the mixing angle between active and sterile neutrinos. The first term accounts for the SM $2\nu\beta\beta$ decay, the second one for the decay in which one of the two neutrinos is replaced by a sterile neutrino (equation (13a) with $f = N$), and the last one for the decay into two sterile neutrinos (equation (13b) with $f = N$). We note here that this last term is strongly suppressed by a factor of $\sin^4 \theta$, making it negligible for experimental searches.

Each term of the sum can be factorized as the product of the NME and the phase space factor:

$$\Gamma_{ab} = |\mathcal{M}_{2\nu}|^2 \, \mathcal{G}_{ab}, \tag{15}$$

where a and b indicate the emitted particles, either the active or the sterile neutrinos. While the NME is the same for the three terms, the phase space factor is affected by the presence of one or two sterile neutrinos in the final state, and so is the summed electron energy distribution:

$$\frac{\mathrm{d}\Gamma_{ab}}{\mathrm{d}K} = |\mathcal{M}_{2\nu}|^2 \, \frac{\mathrm{d}\mathcal{G}_{ab}}{\mathrm{d}K} \tag{16}$$

The presence of a massive sterile neutrino in the final state affects the kinematics of the decay such that the endpoint of the summed electron energy distribution is shifted to $Q_{\beta\beta} - m_N$, where m_N is the sterile neutrino mass.
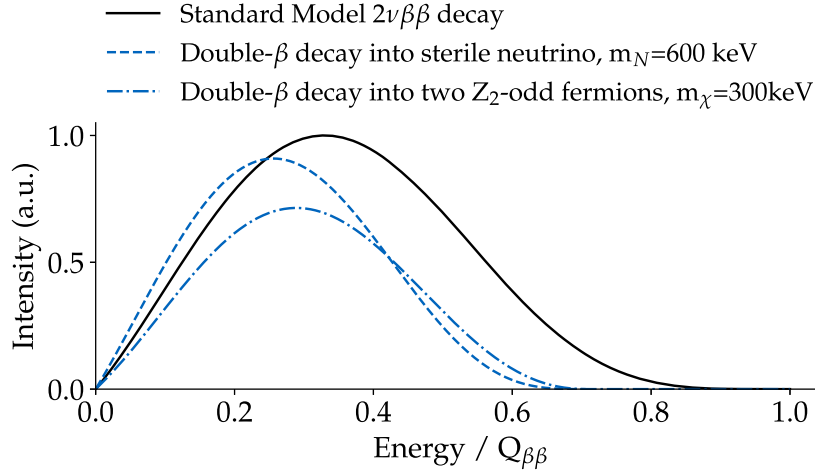
Figure 6. Summed electron energy distributions of the double-β decay into one sterile neutrino with a mass of 600 keV and the double-β decay into two Z_2-odd fermions with a mass of 300 keV in comparison to the SM $2\nu\beta\beta$ decay distribution for the case of ^{76}Ge isotope. The mass of the emitted exotic fermion determines the endpoint of the distribution. The endpoint shifts to the left for larger masses and vice versa. An infinite energy resolution is assumed, and an arbitrary normalization is used for illustrative purposes. Reproduced from [83]. CC BY 4.0.

Z_2-odd fermions, which we refer to as χ fermions, can be produced in double-β decay via the (13b) channel. To be kinematically allowed, the $Q_{\beta\beta}$ value of the decay must be larger than twice the mass of the χ fermions. The rate of the double-β decay with the emission of two fermions χ can be expressed as:

$$\Gamma^{\chi\chi} = \frac{g_\chi^2 \, m_e^2}{8\pi^2 \, R^2} \, |\mathcal{M}^{0\nu}|^2 \, \mathcal{G}^{\chi\chi}, \tag{17}$$

where g_χ is the coupling between neutrinos and the χ fermions, m_e the electron mass, and R the nuclear radius. The NME for this decay can be taken to good approximation as the NME for the $0\nu\beta\beta$ decay, $\mathcal{M}_{0\nu}$. The presence of two massive χ fermions in the final state affects the kinematics of the decay as for the case of sterile neutrinos: the endpoint of the summed electron energy distribution is shifted by $Q_{\beta\beta} - 2m_\chi$, where m_χ is the χ-fermion mass.

Figure 6 shows, for the case of ^{76}Ge isotope, the energy distribution for the double-β decay with the emission of one sterile neutrino with a mass of 600 keV and with two χ fermions with a mass of 300 keV.

3.2. Violation of fundamental symmetries

3.2.1. Lorentz violation.
Lorentz invariance is one of the fundamental symmetries of the SM of particle physics. The breakdown of Lorentz and CPT symmetries at the Plank scale is an interesting feature of many theories of quantum gravity, such as string theory [84]. Although direct studies of physics at this ultrahigh energy scale are far from the reach of current accelerator-based experiments, some suppressed effects could arise at lower energies and be observable with the current experimental technologies.

The general framework that characterizes Lorentz violation in the SM is the SM extension (SME) [85, 86]. This is an effective quantum field theory that includes all possible

operators that can be constructed with the SM fields and that introduce Lorentz violation but preserve the SM gauge invariance. The development of the SME has led to experimental searches for Lorentz violation in different sectors of physics, including matter, photon, neutrino, and gravity [87, 88]. A data table of the current constraints is compiled in [89] annually.

In particular, the SME allows to specify all possible Lorentz-invariance-violating operators for neutrino propagation [90, 91]. Most of these coefficients are currently constrained by neutrino oscillation experiments, which compare how different neutrinos propagate and provide interferometric sensitivity to energy differences between neutrinos [92]. The so-called *oscillation-free* operators, which cannot be assessed via oscillation experiments because they change all neutrino energies equally, are usually constrained by time-of-flight experiments, which match the group velocity of neutrinos with that of photons [92]. However, four oscillation-free operators leave unaffected the neutrino group velocity and so cannot be detected in this way. Instead, they can be accessed through interaction processes that involve the phase space properties of the neutrino, such as weak decays [93–95].

The interaction of neutrinos with the *oscillation-free* operator modifies their four-momentum [94]:

$$p = (E, \boldsymbol{p}) \longrightarrow p = (E, \boldsymbol{p} + \boldsymbol{a}_{of}^{(3)} - \mathring{a}_{of}^{(3)}\hat{\boldsymbol{p}}) \tag{18}$$

where $\boldsymbol{a}_{of}^{(3)}$ encodes the *oscillation-free (of)* coefficients $(a_{of}^{(d=3)})_{jm}$, with j and m denoting the angular momentum quantum numbers with $j = 0, 1$, and d standing for the mass dimension of the corresponding operator. The coefficient $\mathring{a}_{of}^{(3)}$ corresponds to the isotropic component $\mathring{a}_{of}^{(3)} \equiv (a_{of}^{(3)})_{00}/\sqrt{4\pi}$ [94]. Considering this modification, the decay rate of the $2\nu\beta\beta$ decay in the SME framework can be written as the sum of two terms:

$$\Gamma_{\mathrm{SME}}^{2\nu} = \Gamma_{\mathrm{SM}} + \delta\Gamma_{\mathrm{LV}}, \tag{19}$$

where Γ_{SM} is the SM decay rate and $\delta\Gamma_{\mathrm{LV}}$ is the perturbation term due to the introduction of Lorentz violation. Similarly to the previous cases, we can factorize each term as the product of the NME and the phase space factor (see equation (15)). Lorentz violation does not affect the NME but appears as a kinematic effect modifying the phase space factor and, therefore, the summed electron energy distribution:

$$\frac{\mathrm{d}\Gamma_{\mathrm{SME}}^{2\nu}}{\mathrm{d}K} = |\mathcal{M}_{2\nu}|^2 \left(\frac{\mathrm{d}\mathcal{G}_{\mathrm{SM}}}{\mathrm{d}K} + \frac{\mathrm{d}(\delta\mathcal{G}_{\mathrm{LV}})}{\mathrm{d}K} \right) \tag{20}$$

The modification of the phase space $\mathrm{d}(\delta\mathcal{G}_{\mathrm{LV}})/\mathrm{d}K$ comes from the change of the differential element of the anti-neutrino momentum:

$$\mathrm{d}^3p = 4\pi \, E^2\mathrm{d}E \longrightarrow \mathrm{d}^3p = 4\pi \, (E^2 + 2E \, \mathring{a}_{of}^{(3)})\mathrm{d}E. \tag{21}$$

The integration over all anti-neutrino orientation, performed to obtain the summed electron energy distribution in the case of double-β decays, implies that only isotropic effects are observable. Hence, the spectrum only depends on $\mathring{a}_{of}^{(3)}$.

The energy dependency in the phase space of the perturbation term can be approximated as $\delta\mathcal{G}_{\mathrm{LV}} \sim (Q_{\beta\beta} - K)^4$. Using the same terminology introduced for the Majoron, the spectral index of this perturbation is $n = 4$. On the other hand, the spectral index of the SM term is $n = 5$. Therefore, a non-zero value of the coefficient $\mathring{a}_{of}^{(3)}$, which implies a non-zero contribution of the perturbation term, produces a distortion of the spectrum of double-β

decays compared to the SM expectation. The energy distribution of the Lorentz violating perturbation term is shown in figure 7 compared to the SM $2\nu\beta\beta$ decay distribution.

3.2.2. Violation of Pauli exclusion principle. Pauli's original formulation of the exclusion principle in 1925 postulated that two or more identical electrons cannot occupy the same quantum state within a quantum system simultaneously. This was successively formalized into the well-known spin-statistics theorem [96]. According to it, the wave function of integer-spin particles should be symmetric, meaning that it is invariant under permutations of the position of identical particles. Those particles are categorized as bosons, and an ensemble of bosons in thermal equilibrium obeys the Bose–Einstein distribution. On the other hand, particles with half-integer spin should be represented by antisymmetric wave functions, which change sign under position permutations. These particles are named fermions, and their thermal distribution is the Fermi–Dirac distribution. Neutrinos fall in the second category. However, contrary to the case of electrons and nucleons, a possible violation of the Pauli exclusion principle for neutrinos is not yet experimentally excluded.

This possibility and its consequences were investigated in several works. In [97], the authors investigated the effect of the neutrino statistics on the ^{4}He abundance in the early Universe. In [98–100], more cosmological and astrophysical consequences of bosonic neutrinos were investigated. Bosonic neutrinos with masses of a fraction of eV may form a cosmological Bose condensate, which could account for all (or a part of) the dark matter in the Universe [98, 101, 102]. Bosonic neutrinos in the Big Bang nucleosynthesis would lead to the effective number of neutrino species smaller than three [98, 99, 103]. They would also influence the dynamics of the supernova collapse, changing the spectra of the supernova neutrinos [98, 104]. Despite the many cosmological and astrophysical probes, recent analyses of available data can set only weak bounds on neutrino statistics [100].

With two identical anti-neutrinos in the final state, double-β decay is a unique process to test the violation of Pauli's principle [99, 105]. Qualitative conclusions in [99] on $2\nu\beta\beta$ decay ruled out a pure bosonic neutrino, but not the possibility that neutrinos obey non-standard statistics, more general than Bose or Fermi ones [106].

If neutrinos obey a mixed statistic, the neutrino's state would be the combination of fermionic and bosonic states. The $2\nu\beta\beta$ decay rate can be written as:

$$\Gamma_{2\nu\beta\beta} = \cos^4\chi\,\Gamma_f + \sin^4\chi\,\Gamma_b, \tag{22}$$

where Γ_f and Γ_b are the decay rates calculated for purely fermionic neutrinos and purely bosonic neutrinos, respectively, and $\sin^4\chi$ is a parameter which embeds the mixing between the two states. The change from purely fermionic to purely bosonic neutrinos affects both the kinematic term and the NME. Defining the ratio

$$r_0 = \Gamma_b/\Gamma_f, \tag{23}$$

the normalized differential decay rate can be written as

$$\frac{d\Gamma_{\text{tot}}}{\Gamma_{\text{tot}}} = \frac{\cos^4\chi}{\cos^4\chi + \sin^4\chi\,r_0}\frac{d\Gamma_f}{\Gamma_f} + \frac{\sin^4\chi\,r_0}{\cos^4\chi + \sin^4\chi\,r_0}\frac{d\Gamma_b}{\Gamma_b}. \tag{24}$$

The ratio r_0 determines the weight with which the bosonic component enters the total rate and the differential decay distribution. If r_0 is very small, a substantial modification of the energy distribution is expected only for $\sin^2\chi$ being very close to 1. In addition, the ratio r_0 needs to be calculated and depends on the values of the NMEs. Thus, it introduces an uncertainty due to the nuclear-structure calculations.
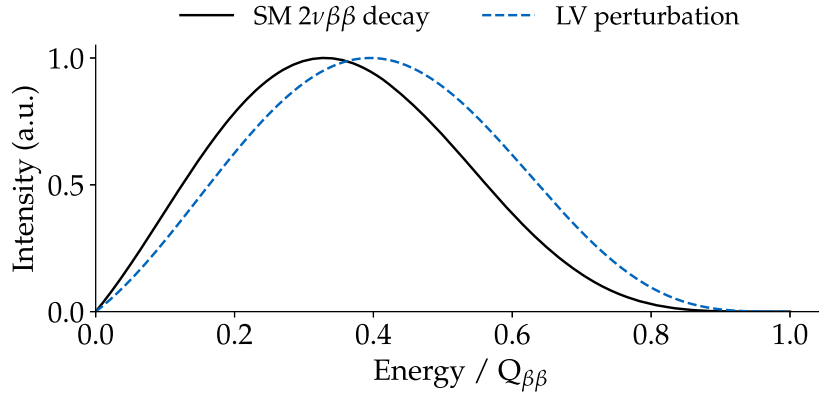
Figure 7. Summed electron energy distribution of the $2\nu\beta\beta$ decay in the SM and the perturbation term introduced by Lorentz violation (LV) for the isotope ^{76}Ge. An infinite energy resolution is assumed, and an arbitrary normalization is used for illustrative purposes.

On the other hand, the normalized differential decay rate for pure fermionic $d\Gamma_f/\Gamma_f$ and pure bosonic $d\Gamma_b/\Gamma_b$ neutrinos does not depend on any nuclear model assumption and is shown in figure 8. The spectrum for bosonic neutrinos is softer, with the maximum shifted to lower energy by a factor of about 15%, compared to the pure fermionic spectrum.

Calculations of the NMEs were performed in [105] for the isotopes ^{100}Mo and ^{76}Ge. In the case of ^{100}Mo, calculations were conducted under the single state dominance hypothesis, using existing experimental data for the β decay and the electron capture of ^{100}Tc, which is the intermediate dominating state. The authors predicted a value of the ratio $r_0 = 0.076$. In the case of ^{76}Ge, calculations were conducted under the Higher State Dominance hypothesis within the proton-neutron QRPA framework and predicted a value of the ratio $r_0 = 0.0014$. The small ratio predicted for ^{76}Ge limits the sensitivity of double-β decay experiments with ^{76}Ge to spectral distortions due to a partly bosonic neutrino.

3.3. Non-standard interactions

3.3.1. Right-handed leptonic currents. The SM $2\nu\beta\beta$ decay is a second-order transition involving weak left-handed V–A currents with the strength given by the Fermi constant G_F. Some BSM theories, such as Left–Right symmetric models with unbroken lepton number [107, 108], predict the existence of V + A lepton currents, which can mediate double-β decays [109]. The new physics effects can be modeled through effective charged current operators containing V + A lepton currents. The strength of these non-standard interactions is given by $\epsilon_{XR} G_F$, where the small dimensionless coupling ϵ_{XR} encapsulates the new physics effects.

Right-handed current interactions are independent of the Majorana or Dirac nature of neutrinos and do not necessarily violate the lepton number symmetry. If the neutrino were Majorana particle, the operators associated with ϵ_{LR} and ϵ_{RR} would violate the total lepton number by two units and give rise to extra contributions to the $0\nu\beta\beta$ decay [42]. This case is strongly constrained by existing $0\nu\beta\beta$ decay limits at the order $\epsilon_{LR} \lesssim 3 \times 10^{-9}$, $\epsilon_{RR} \lesssim 6 \times 10^{-7}$ [110]. The right-handed nature of the interaction can also be accommodated in another way, namely by the existence of a separate right-handed neutrino state, which is sterile under the SM gauge interactions but participates in non-standard interactions. In the
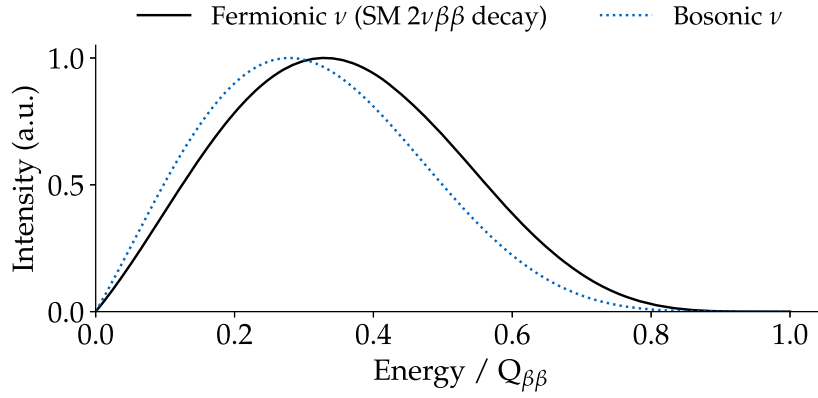
Figure 8. Summed electron energy distribution of the $2\nu\beta\beta$ decay for pure bosonic neutrinos compared to the case of pure fermionic neutrinos (SM $2\nu\beta\beta$ decay) for the isotope ^{76}Ge. An infinite energy resolution is assumed, and an arbitrary normalization is used for illustrative purposes.

latter case, the lepton number is conserved and the neutrinos are expected to be Dirac fermions. The strong theoretical interest in such right-handed leptonic currents is therefore supported by the fact that their observation, together with the non-observation of lepton number violation, would indicate that neutrinos are Dirac fermions [108].

Experimental constraints on these operators are established through fitting data from neutron lifetime experiments and various single-β decay experiments; however, these constraints are relatively weak ($\epsilon_{\text{LR}}, \epsilon_{RR} \lesssim 6 \times 10^{-2}$) [111, 112]. Searches at the LHC are also possible [113–115] but are generally model-dependent and require some caveat on the use of the effective operator analysis at high energies [112].

In the presence of right-handed leptonic currents, the amplitude of the $2\nu\beta\beta$ decay would be calculated as a coherent sum of the three Feynman diagrams shown in figure 9: the SM second-order transition with two left-handed interactions with the strength given by G_F^2 (figure 9(a)), a transition involving one right-handed interaction with strength $\epsilon_{XR} G_F^2$ (figure 9(b)), and a second-order transition with two right-handed interactions with strength $\epsilon_{XR}^2 G_F^2$ (figure 9(c)). Nevertheless, to the lowest order in the exotic coupling ϵ_{XR}, the decay rate can be expressed as an incoherent sum of only two terms:

$$\Gamma^{2\nu} = \Gamma_{\text{SM}} + \epsilon_{XR}^2\, \Gamma_\epsilon, \tag{25}$$

where the first term is the SM decay rate and the second term is the contribution of right-handed current to the decay rate, suppressed by the coupling ϵ_{XR}. In fact, the interference of the SM term (diagram 9(a)) with diagram 9(b) is helicity suppressed by the masses of the emitted electron and neutrino as $m_e m_\nu / Q_{\beta\beta}^2$ because of the right-handed nature of the exotic current. Higher orders in the exotic coupling ϵ_{XR}, coming from the last diagram 9(c) and its interference with the SM term, are also negligible.

The phase-space factor and the NME differ in the SM decay rate and the BSM contribution. Thus, the presence of right-handed currents in double-β decay changes the total decay rate and the shape of the energy spectrum. Nevertheless, given the uncertainties in the NME calculations, the change in the total decay rate is not expected to be measurable. Instead, experiments may be sensitive to the change in the spectral shape. Figure 10 shows the decay distribution of the $2\nu\beta\beta$ decay in the SM alongside the distribution resulting from the introduction of right-handed currents for the isotope ^{100}Mo. The latter distribution is
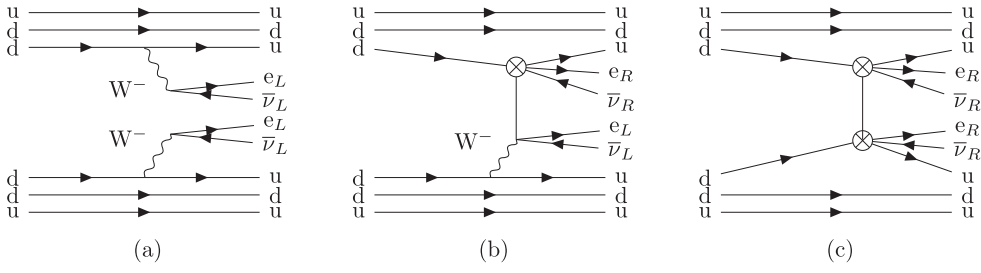
Figure 9. Feynman diagrams of the double-β decay (a) with two left-handed currents, i.e. the SM $2\nu\beta\beta$ decay, (b) with one right-handed current, and (c) with two right-handed currents. Reproduced from [109]. CC BY 4.0.
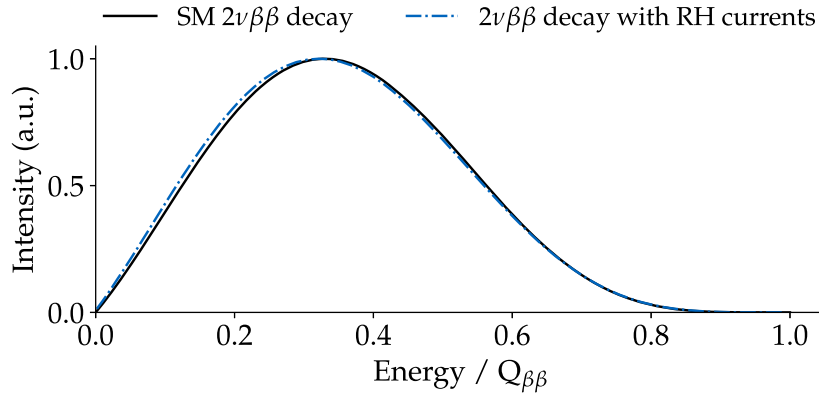

Figure 10. Summed electron energy distribution of the $2\nu\beta\beta$ decay in the presence of right-handed lepton currents compared to the SM $2\nu\beta\beta$ decay (left-handed lepton currents) for the ^{100}Mo isotope. An infinite energy resolution is assumed, and an arbitrary normalization is used for illustrative purposes. Reproduced from [109]. CC BY 4.0.

displayed without any assumption on the parameter ϵ_{XR}, and it is normalized arbitrarily. The primary objective here is to emphasize the distinctions in the distribution's shape between these two scenarios. This deviation is characterized by a shift of the spectrum to smaller energy and a flatter profile near $Q_{\beta\beta}$.

3.3.2. Neutrino self-interaction. There is a discrepancy between the locally measured value of the Hubble constant and the value predicted by the SM of cosmology (ΛCDM model) calibrated using Planck CMB data [116–118]. This $\sim$9% discrepancy has grown to about 4σ level and is widely referred to as the 'Hubble Tension'. If confirmed, it would require new physics BSM or a new ΛCDM model [119].

Introducing a neutrino self-interaction (νSI), i.e. a four-neutrino contact interaction, could resolve the Hubble tension [120, 121]. Such a νSI can be written as $G_S(\nu\nu)(\nu\nu)$, and it would inhibit neutrino free-streaming in the early Universe if its strength is much larger than the Fermi effective interaction predicted by the SM, $G_S \sim 10^9$ G$_F$ [120, 121]. This new strong interaction would indicate the presence of new physics at a scale $1/\sqrt{G_S} \sim 10\,\text{MeV}$–$1\,\text{GeV}$. In general, these strong νSI are difficult to probe in laboratory experiments due to the absence of electrons or quarks. With some assumption on the origin of the νSI operator, constraints
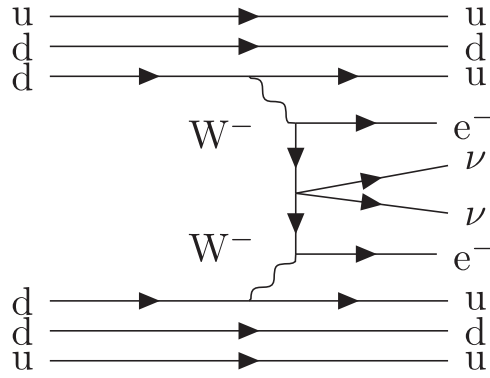
Figure 11. Feynman diagram of the double-β decay induced by νSI. Reproduced from [125]. CC BY 4.0.

can be obtained from different physics observations [122, 123], while no model-independent constraint is currently available. The study of νSI in single-β decays has been considered [124]. More recently, the search for νSI in double-β decays has also been proposed [125].

In the presence of νSI, independently of the Dirac/Majorana nature of neutrinos, the two neutrinos in double-β decay can be emitted via the corresponding effective operator, resulting in a νSI-induced $2\nu\beta\beta$ (2νSI$\beta\beta$) decay. The Feynman diagram of this process is shown in figure 11. The final state of the 2νSI$\beta\beta$ decay is identical to that of the SM $2\nu\beta\beta$ decay. The contribution from νSI to the decay rate can be written as:

$$\Gamma_{\nu\mathrm{SI}} = \frac{G_S^2 m_e^2}{4R^2} \, \mathcal{G}_{\nu\mathrm{SI}} \, |\mathcal{M}_{0\nu}|^2, \tag{26}$$

where m_e denotes the electron mass and R the radius of the nucleus. For an exact contact interaction of four neutrinos and neglecting the final state lepton momenta, the phase-space factor for the 2νSI$\beta\beta$ decay is related to the phase-space factor of the $2\nu\beta\beta$ decay by $\mathcal{G}_{\nu\mathrm{SI}} = \mathcal{G}_{2\nu}/(4\pi)^2$. The NME of 2νSI$\beta\beta$ is the same as of $0\nu\beta\beta$. In this scenario, no difference is expected in the summed electron energy distribution of the 2νSI$\beta\beta$ decay compared to the SM $2\nu\beta\beta$ decay. Therefore, only the experimental measurements of the $2\nu\beta\beta$ decay rate can be used to constrain the contribution of νSI.

This approach was used in [125] to determine upper limits on the coupling G_S from the measured $2\nu\beta\beta$ decay rates of several double-β decay isotopes. The authors derived constraints within the range $G_S/G_F \lesssim (0.32-2.50) \times 10^9$, reflecting the considerable uncertainty in the NME ratio $|\mathcal{M}_{0\nu}|/|\mathcal{M}_{2\nu}|$. Despite incorporating theoretical uncertainties of the NMEs, all examined isotopes unequivocally rule out the strongly interacting regime preferred by cosmological data, where $G_S = 3.83 \times 10^9 \, G_F$. However, one should note that this bound applies only under the assumption that two-electron neutrinos are involved in the νSI. This might not be the case if only muon neutrinos and tau neutrinos participate in νSI [125].

Possible distortions of the electron energy distribution could arise from the νSI contribution if the νSI operator were generated by light mediators. In this scenario, the energy dependence of the coupling G_S could cause observable spectral distortions. In [125], the simplest case of an s-channel scalar mediator with a mass just above the kinematic threshold ($M = Q_{\beta\beta} + 0.1m_e$) was discussed. The coupling G_S acquires the following energy dependence
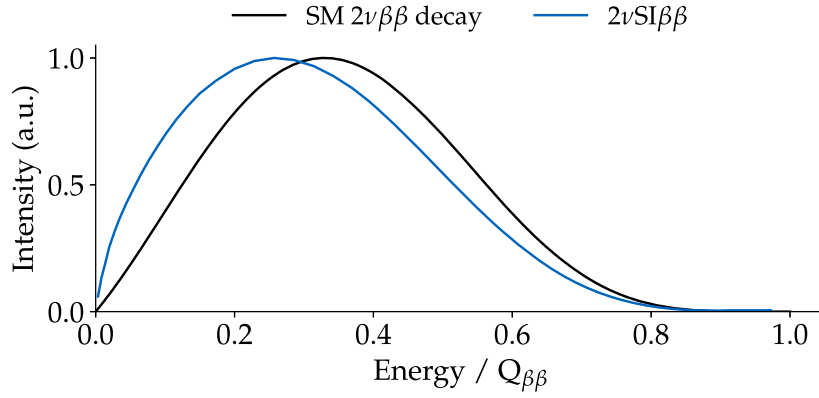
Figure 12. Summed electron energy distribution of $2\nu\mathrm{SI}\beta\beta$ decay where the $\nu\mathrm{SI}$ operator is generated by an s-channel mediator with a mass of $M = Q_{\beta\beta} + 0.1 m_e$, compared to the SM $2\nu\beta\beta$ decay for the ^{100}Mo isotope. An infinite energy resolution is assumed, and an arbitrary normalization is used for illustrative purposes. Reproduced from [125]. CC BY 4.0.

$$G_S = \frac{-M^2}{s - M^2} \, G_S^0, \tag{27}$$

where M is the mediator mass and $s \equiv p^2$, with p being the momentum of the mediator (in the context of the $2\nu\mathrm{SI}$ $\beta\beta$, this is of the order $s \lesssim Q_{\beta\beta}^2$). The value of G_S at zero momentum transferred (G_S^0) is denoted as $G_S^0 = g^2/M^2$, with g the coupling between the mediator and the neutrino. Using G_S in equation (27), the differential decay rate of the $2\nu\mathrm{SI}\beta\beta$ decay can be calculated. The corresponding summed electron energy distribution is shown in figure 12, for a mass of the mediator $M = Q_{\beta\beta} + 0.1 m_e$. The energy spectrum of the $2\nu\mathrm{SI}\beta\beta$ decay is shifted at lower energy compared to the $2\nu\beta\beta$ decay spectrum. This shift can be understood qualitatively: with the summed energy of the two electrons increasing, the energy available for the neutrinos is smaller, leading to a smaller value of s and hence a smaller value of G_S.

4. Statistical signal extraction and sensitivity

All the double-β decays introduced in section 3 result in the same event topology. The two electrons emitted in the decay are detected within the detector volume. The additional particles produced in the double-β decay process, either the two anti-neutrinos or one or more exotic particles, escape the detector, carrying away part of the decay energy.

Double-β decay experiments typically measure multiple observables for each event. These include, for instance, the energy deposited within the detector, spatial and timing information, and variables related to the type of particles involved in the event. Signal and background events feature specific values of these observables that can be used to separate them. As previously mentioned, this review focuses on discovery opportunities based on the measurement of the summed energy of the two electrons emitted in the decay, as this is the only kinematic observable to which leading $0\nu\beta\beta$ decay searches will be sensitive in the next decade. The potential impact of measuring other observables of the decay kinematics, such as single-β energy spectra and opening angle distributions, will be briefly covered in section 4.6.

Before discussing the statistical analysis to search for BSM decays, we shall divide them into three classes of models, which require slightly different statistical treatments.
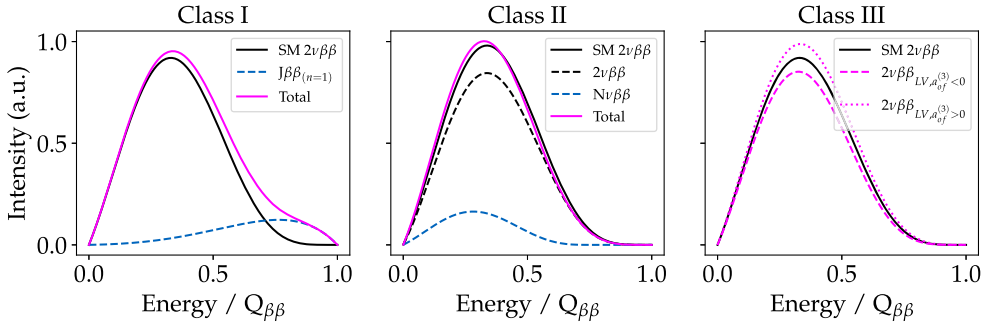
Figure 13. The three classes of BSM double-β decay models.

Class I models. The first class contains all those BSM decays whose rate and kinematic is decoupled by the SM $2\nu\beta\beta$ decay, and so there is no correlation in term of phase space or NME between the two processes. This is the case for decays involving Majorons (3.1.1), Z_2-odd massive fermions (second model in 3.1.2), and $2\nu\beta\beta$ decay realized via non-standard interaction when interference terms are negligible (3.3). All these processes would manifest as an independent contribution to the total energy spectrum, i.e. a continuous distribution in the same energy range of the SM $2\nu\beta\beta$ decay. As we expect BSM processes to be suppressed at this energy scale, only minor spectral distortions are expected compared to the pure SM expectation. This is shown in the left panel of figure 13, for the illustrative case of a J$\beta\beta$ decay ($n = 1$) in ^{76}Ge with a non-realistically large coupling $g_J \sim 2 \times 10^{-4}$. In the search for such a BSM decay, the parameter of interest is the integrated number of BSM decay events, and the $2\nu\beta\beta$ decay events act as background.

Class II models. The second class contains those models that are in competition with the SM $2\nu\beta\beta$ decay, so their existence would result in a relative reduction of the $2\nu\beta\beta$ decay rate. In the search for such a BSM decay, the parameter of interest is proportional to the ratio between the integral number of BSM decay events and the integral number of $2\nu\beta\beta$ decay events. This is typically a 'mixing' parameter, such as $\cos^4 \theta$ for models with sterile neutrinos (see section 3.1.2), or $\cos^4 \chi$ for models with bosonic neutrinos (see section 3.2.2). The central panel of figure 13 captures these scenarios, showing the illustrative case of ^{76}Ge decays with a sterile neutrino with mass $m_N = 500$ keV and a large mixing of $\sin^2 \theta = 0.15$, as an example. Assuming that BSM physics is suppressed at these energy scales, only minor spectral distortions of the energy spectrum are expected compared to the pure $2\nu\beta\beta$-decay SM. From the statistical point of view, the higher the summed rate, the higher the statistics and, in turn, the sensitivity to observe spectral. Thus, isotopes with shorter $2\nu\beta\beta$-decay half-life values will be favorable, as formalised later in section 4.3.

Class III models. The third class of models we consider includes those altering the SM $2\nu\beta\beta$ decay itself, e.g. modifying its kinematic or rate without introducing additional decay channels. The violation of Lorentz symmetry is the only model considered in this review that falls into this class. Indeed, the Lorentz violating term in the neutrino momentum affects the phase space of the two electrons emitted in the $2\nu\beta\beta$ decay and, therefore, the predicted energy distribution. This is shown in the right panel of figure 13, for the illustrative case of ^{76}Ge decaying with non-realistically large values of the Lorentz violating coefficient $|\mathring{a}_{of}^{(3)}| \sim 10^{-4}$. Thus, the search for Lorentz violation in $2\nu\beta\beta$ decays corresponds to a search for deviations in the two-electron energy distribution compared to the SM expectation. However, in practical terms, Lorentz violations can be traced back to a Class II model in

which the Lorentz violating effects are treated as a perturbation of the SM $2\nu\beta\beta$-decay spectrum, and the Taylor expansion is truncated to the first order [94]. The parameter of interest in this treatment becomes the ratio between the number of events underlying the distribution of the LV perturbation (i.e. the first term of the expansion) and the number of events underlying the SM $2\nu\beta\beta$ decay distribution (i.e. the leading term). As for all other Class II models, the larger the $2\nu\beta\beta$-decay event sample, the lower the statistical uncertainties and the higher the sensitivity to deviations.

4.1. Statistical signal extraction

In the search for spectral distortions due to the contribution of a BSM decay in the energy spectrum, the energy region of interest extends from the detector threshold to $Q_{\beta\beta}$. In this window, most of the observed events are attributed to the $2\nu\beta\beta$ decay $N_{2\nu}$ with additional contributions due to different background processes N_{others}. The sum of the $2\nu\beta\beta$ decay and other background constitutes the so-called background model, which is known with a certain accuracy by the experiments.

To search for a BSM decay, a spectral fit of the energy spectrum is performed,[6] adding the BSM decay to the background model. Typically, the information from the background model is used to construct a likelihood function, which is then used in a frequentist or Bayesian approach to constrain the parameter of interest. The definition of the parameter of interest depends on the model to be constrained, as was pointed out in the previous section.

The most important experimental parameters determining the sensitivity of the experiment are the exposure $\mathcal{E}$, the background rate R_{bkg}, the signal detection efficiency ε, and the systematic uncertainties σ_{sys}. The exposure is given by the product of the number of observed nuclei and the observation time. The background rate is primarily given by the $2\nu\beta\beta$ decay rate with a subdominant contribution due to other sources $R_{bkg} = R_{2\nu} + R_{\text{others}}$. The signal detection efficiency refers to the probability of a signal event being detected and surviving all analysis cuts. We assume this to be not energy dependent and only to affect the total number of observed events. Overall detection efficiency uncertainties are typically negligible unless they introduce an energy-dependent bias affecting the shape of the summed electron energy distribution. We encompass this effect as part of the systematic uncertainties. The systematic uncertainties can largely differ between experiments and are specific to the detector technology. In general, in the search for spectral distortion, the most critical systematic uncertainties are those that introduce energy-dependent effects, e.g. uncertainty on the energy reconstruction or any energy-dependent efficiency.

A precise evaluation of the sensitivity of an experiment requires considering experiment-specific information. However, it can be approximated by considering a counting analysis and Poisson statistics in the region of interest defined above and with a known background expectation given by R_{bkg}. In this derivation, we neglect the systematic uncertainties. Their impact will be discussed later in this section. The dependence of the sensitivity on exposure $\mathcal{E}$ and background rate R_{bkg} is different from class I models and class II and III models. In the following, we will discuss the two cases separately.

---

[6] Some experiments utilize a multivariate approach, fitting multiple observables at the same time to better separate signal and background. Here we focus on the simplest approach of one-dimensional fit, but the results can be easily generalized.

4.2. Experimental sensitivity for class I models

Let's first consider a BSM decay which we classified as a class I model. This is, for example, the case of the existence of an exotic particle, e.g. the Majoron or the Z_2-odd exotic fermion, with a coupling to neutrino given by g_X.[7] This is the parameter of interest we want to determine the sensitivity.

The precision with which a subdominant contribution—the number of BSM decays, N_X—can be constrained is proportional to the fluctuations of the background in the analysis window, N_{bkg}:

$$\sigma_{N_X} \propto \sqrt{N_{bkg}}, \tag{28}$$

where the number of background events in the analysis window can be expressed as a function of the background rate and the exposure:

$$N_{bkg} = R_{bkg} \cdot \mathcal{E}. \tag{29}$$

The parameter of interest g_X can be expressed as a function of the number of BSM decays through the phase-space factor $\mathcal{G}$ and the NME $\mathcal{M}$:

$$g_X^2 = \frac{N_X}{\mathcal{G}\,\mathcal{M}^2 \cdot \mathcal{E}}. \tag{30}$$

Using equations (29) and (30) into equation (28), we obtain:

$$\sigma_{g_X^2} \propto \sqrt{\frac{R_{2\nu} + R_{\text{others}}}{\mathcal{E}}} \cdot \frac{1}{\mathcal{G}\,\mathcal{M}^2}. \tag{31}$$

In the last step, we equated the contribution of the $2\nu\beta\beta$ decay to the total background rate $(R_{bkg} = R_{2\nu} + R_{\text{others}})$.

The sensitivity scales with the square root of the exposure, but it is limited by the background, to which the $2\nu\beta\beta$ decay contributes. In addition, equation (31) shows that uncertainties in the phase space and NMEs can limit the sensitivity.

4.3. Experimental sensitivity for class II and III models

A slightly different result is obtained for class II and III models. Let's consider, for instance, the double-β decay into sterile neutrinos.[8] In this case, the parameter of interest is the mixing angle $\sin^2\theta$. Given that $\sin^2\theta$ also modifies the $2\nu\beta\beta$ decay rate, it is proportional to the ratio between the number of decays into sterile neutrino $N_{\nu N}$ and the number of $2\nu\beta\beta$ decay events

$$\sin^2\theta \propto \frac{\mathcal{G}_{2\nu}}{\mathcal{G}_{\nu N}} \cdot \frac{N_{\nu N}}{N_{2\nu}}, \tag{32}$$

through the respective phase-space factors.

The statistical uncertainty on this quantity can be computed through standard error propagation

$$\frac{\sigma_{\sin^2\theta}}{\sin^2\theta} \propto \left\{ \left(\frac{\sigma_{N_{\nu N}}}{N_{\nu N}} \right)^2 + \left(\frac{\sigma_{N_{2\nu}}}{N_{2\nu}} \right)^2 + 2 \cdot \left(\frac{\sigma_{N_{\nu N}} \sigma_{N_{2\nu}}}{N_{\nu N} N_{2\nu}} \right) \rho_{N_{\nu N}, N_{2\nu}} \right\}^{1/2}. \tag{33}$$

---

[7] The result can be extended to the existence of non-standard interaction, which leads to BSM double-β decays, as introduced in section 3.3.
[8] The result can be extended to the double-β decay into bosonic neutrinos and the Lorentz violating $2\nu\beta\beta$ decay.

Because of the same arguments previously used to define the uncertainty on N_X, the uncertainty on $N_{\nu N}$ will be

$$\sigma_{N_{\nu N}} \propto \sqrt{(R_{2\nu} + R_{\text{others}}) \cdot \mathcal{E}}. \tag{34}$$

In addition, we can write $N_{\nu N}$ in terms of $N_{2\nu}$ and $\sin^2\theta$. Also, the correlation coefficient $\rho_{N_{\nu N}, N_{2\nu}}$ is proportional to the mixing angle, because of the relation (32). Putting everything together, we can rewrite equation (33) as:

$$\frac{\sigma_{\sin^2\theta}}{\sin^2\theta} \propto \left\{ \frac{(R_{2\nu} + R_{\text{others}}) \cdot \mathcal{E}}{R_{2\nu}^2 \cdot \sin^4\theta \cdot \mathcal{E}^2} + \frac{1}{R_{2\nu} \cdot \mathcal{E}} + 2 \cdot \frac{\sqrt{R_{2\nu}(R_{2\nu} + R_{\text{others}})} \cdot \mathcal{E}}{R_{2\nu}^2 \cdot \sin^2\theta \cdot \mathcal{E}^2} \right\}^{1/2}, \tag{35}$$

$$\sigma_{\sin^2\theta} \propto \left\{ \frac{(R_{2\nu} + R_{\text{others}})}{R_{2\nu}^2 \cdot \mathcal{E}} + \frac{\sin^4\theta}{R_{2\nu} \cdot \mathcal{E}} + \frac{2 \cdot \sin^2\theta \sqrt{R_{2\nu}(R_{2\nu} + R_{\text{others}})}}{R_{2\nu}^2 \cdot \mathcal{E}} \right\}^{1/2}, \tag{36}$$

$$\sigma_{\sin^2\theta} \rightarrow \sin^2\theta \sim 0 \mathcal{G}_{2\nu}/\mathcal{G}_{\nu N} \cdot \sqrt{\frac{(R_{2\nu} + R_{\text{others}})}{R_{2\nu}^2 \cdot \mathcal{E}}}, \tag{37}$$

where we reintroduced the dependence on the phase-space factors in the last passage.

The sensitivity scales with the square root of the exposure, it is limited by the background, but in this case, a high $2\nu\beta\beta$ decay rate is advantageous due to the dependence $\sigma_{\sin^2\theta} \propto \sqrt{1/R_{2\nu}}$. The sensitivity also depends on the ratio between the phase space factors $\mathcal{G}_{2\nu}/\mathcal{G}_{\nu N}$.

4.4. Impact of the systematic uncertainties on the sensitivity

Given an experiment with exposure $\mathcal{E}$ and using an isotope with half-life $T_{1/2}^{2\nu}$, we expect the sensitivity to double-β decay into Majorons or Z_2-odd fermions (or decays resulting from non-standard interaction) to scale with $\sqrt{1/(T_{1/2}^{2\nu} \cdot \mathcal{E})}$ while the sensitivity to the sterile neutrino mixing angle (or Lorentz violation and bosonic neutrinos) with $\sqrt{T_{1/2}^{2\nu}/\mathcal{E}}$. This means that experiments using an isotope with a long $2\nu\beta\beta$ decay half-life will be favored in the first kind of search as they will have a lower background rate. However, they will be disfavoured in the second kind of search where the sensitivity is linearly proportional to the $2\nu\beta\beta$ decay half-life.

In our derivation so far, we have neglected the impact of systematic uncertainties on the sensitivity. In a more general way, the sensitivity can be approximated as

$$f(\mathcal{E}, R_{bkg}, \sigma_{\text{sys}}) = \sqrt{\sigma_{\text{stat}}^2(\mathcal{E}, R_{bkg}) + \sigma_{\text{sys}}^2}. \tag{38}$$

It is determined by both the statistical uncertainty σ_{stat}, which was derived in equations (31) and (37) as a function of the most important experimental parameters, and the systematic uncertainty σ_{sys}.

As long as the statistical uncertainty is dominant, the sensitivity improves by increasing the exposure approximately as $f \propto \sqrt{1/\mathcal{E}}$. The sensitivity saturates when the statistical uncertainty becomes comparable with the systematic one. This is illustrated in figure 14, adapted from [83].

In the latter, the authors calculated the sensitivity of a mock double-β decay experiment using ^{76}Ge, with an overall detection efficiency of 75%, to sterile neutrinos with a mass of 500 keV. The sensitivity is shown as a function of the exposure, the background level, and the systematic uncertainties. Systematic uncertainties were parametrized with a generic energy-dependent function $f(E) = 1 + a \cdot E + b \cdot E^2 + c/E$, where a, b, and c are parameters assumed
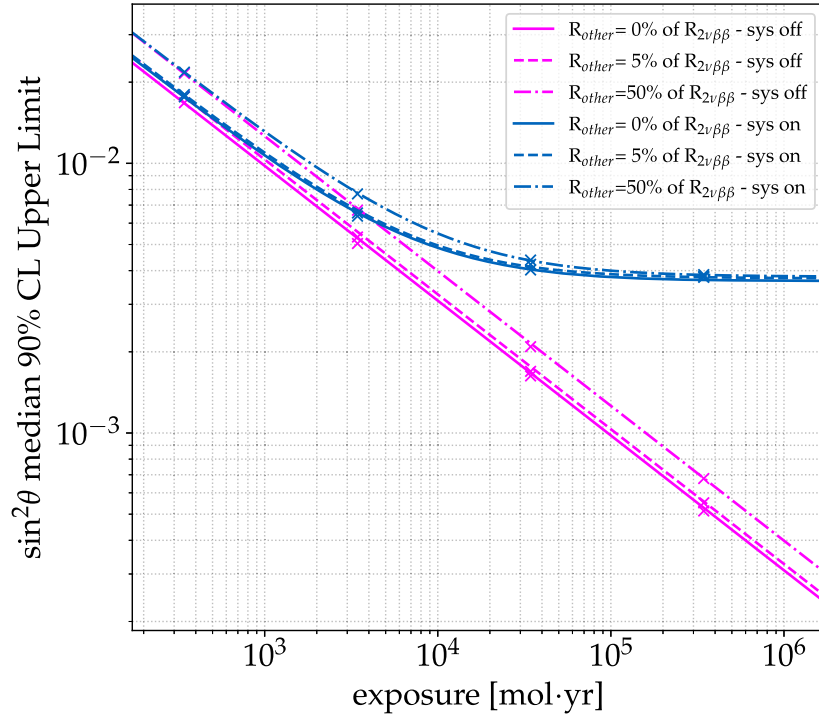
Figure 14. Sensitivity of a double-β decay experiment with ^{76}Ge to sterile neutrinos with a mass of 500 keV, as a function of the exposure, background level, and systematic uncertainties [83]. The results of a full frequentist analysis (markers) are compared to the expectation (lines) from equations (38) and (37).

to be zero with a certain uncertainty given by $\sigma_a = 10^{-3}\,\text{keV}^{-1}$, $\sigma_b = 10^{-6}\,\text{keV}^{-2}$, and $\sigma_c = 10^{-3}\,\text{keV}$, respectively. These specific values were chosen to reproduce the percent-level energy-dependent biases typical of existing experiments. The markers show the sensitivity computed in [83] using a full frequentist analysis. This is compared to the expectation given by equation (38), where the statistical uncertainty is given by equation (37).

4.5. Impact of the NMEs on the sensitivity

As shown by equations (11a), (17), and 26, the NME plays a crucial role when converting the measured quantity into the parameter of interest, for instance, the half-life of the decay into the coupling of a new particle to neutrinos. The NME accounts for the nuclear aspects related to the transition, and its estimation requires challenging many-body calculations of the overlap between the wave functions on the initial and final isotope state, as well as the lepton-nucleus iterations.

Historically, two fundamental many-body methods, the nuclear shell model (NSM) and the quasiparticle random phase approximation (QRPA), have been widely employed for evaluating NMEs for the $0\nu\beta\beta$ and $2\nu\beta\beta$ decays. Additional methods, including the interacting boson model (IBM) and the energy density functional (EDF) method, have been explored for $0\nu\beta\beta$ decay, with recent advancements introducing *ab initio* calculations for the $0\nu\beta\beta$ decay. Significant variations, about a factor of three, exist in NME calculations using different methods for $0\nu\beta\beta$ decay, reflecting uncertainties arising from approximate solutions to the

nuclear many-body problem. Efforts are ongoing to enhance the reliability of these calculations and evaluate their uncertainties, particularly motivated by a potential discovery of $0\nu\beta\beta$ decay in future experiments. We refer to [126] for a comprehensive review on the subject and to [7] for more recent developments in the field.

Compared to the $0\nu\beta\beta$ decay case, only a very limited number of NME calculations is typically available for BSM double-β decays discussed in this review. This does not affect searches focused on distortions of the energy distribution shape but introduces additional systematic uncertainties for the estimation of the half-life or rates of new processes manifesting on the top of the $2\nu\beta\beta$-decay signal.

For the search of Majorons with $n = 1$, the NMEs are the same as for the $0\nu\beta\beta$ decay. As anticipated above, various calculations in different nuclear models yield a range of NME values, translating into a corresponding range of values of the parameter g_J that can be constrained (see table 3). This scenario also applies to the decay with two Z_2-odd light fermions and the double-β decay induced by νSIs. In the case of the Majoron model with $n = 2$, no estimations of phase space or NMEs are currently available. For Majoron models with $n = 3$ and $n = 7$, earlier calculations with large uncertainties and outdated methods [69] have been superseded by recent work [71], which employed the IBM many-body method with isospin restoration.

Decays with right-handed currents, as well as those involving bosonic neutrinos, necessitate NME values to convert the measured quantities into the respective parameters of interest. Calculations in the QRPA formalism are performed for the first scenario in [109] for ^{76}Ge, ^{82}Se, ^{100}Mo, and ^{136}Xe. For the second scenario, calculations in the same framework were performed in [105] for ^{76}Ge and ^{100}Mo.

For the last two BSM decays considered in this review, involving sterile neutrinos and Lorentz violation, the constraints on their respective parameters do not rely on NME calculations. Here, NMEs can be assumed to be the same as in $2\nu\beta\beta$ decay, factoring out in the ratio between the number of BSM decays and $2\nu\beta\beta$ decays to which the parameter of interest is proportional (see section 4.3).

So far, the estimation of NME calculations for the aforementioned searches has not been a priority. However, the development of *ab initio* techniques driven by $0\nu\beta\beta$-decay physics is setting the foundation for precise calculations in any double-β decay transition. Thus, should a hint for new physics manifest in a specific channel, accurate NME estimation will surely become available quickly and will not represent the dominant systematic uncertainty of future experiments.

4.6. Beyond a pure calorimetric measurement of two-electron summed energy

This review focuses on the searches for BSM physics based on the measurement of the summed energy of the two electrons emitted in double-β decay transitions. This choice is motivated by the fact that the future leading experiments in the field (i.e. those that will collect the highest-statistic samples of double-β decays for each isotope and thus be at the forefront of discoveries) are sensitive only to two-electron summed energy.

Nevertheless, it is noteworthy that alternative detection concepts able to extract further info about decay kinematics are being actively pursued, with the goal of following up on potential discoveries with a more complete measurement of the process properties. Although the primary motivation to develop such technologies is to pin down the lepton-violating mechanism driving $0\nu\beta\beta$ decay, exciting discovery opportunities will also arise in the framework of the searches discussed in this review [53, 71, 82, 109, 125, 127, 128]. In particular, depending on the resolution with which these additional observables can be measured,

J. Phys. G: Nucl. Part. Phys. **51** (2024) 023001

Topical Review

Table 3. Comparison of the results obtained by different double-β decay experiments with different isotopes in the search for Majorons-involving decays. The lower limits on the half-life are converted into upper limits on the neutrino-Majoron coupling constant using equation (11a) with the axial vector coupling constant $g_A = 1.27$ and the phase space factors from [70]. The NME calculations for the spectral index $n = 1$ are taken from [7] and references therein, and for $n = 3$ and $n = 7$ from [71].

Decay/Isotope	$T_{1/2}$ (yr)	Experiment	G (10^{-18} yr^{-1})	NME	g_J
J$\beta\beta(n=1)$					
^{48}Ca	$>4.6 \times 10^{21}$	NEMO-3 [39]	1540	$(0.40-2.71)$	$<(8.5-58) \times 10^{-5}$
^{76}Ge	$>6.4 \times 10^{23}$	GERDA [139]	44.2	$(2.66-6.64)$	$<(1.8-4.4) \times 10^{-5}$
^{82}Se	$>3.7 \times 10^{22}$	NEMO-3 [165]	361	$(2.72-5.30)$	$<(3.2-6.2) \times 10^{-5}$
^{82}Se	$>1.2 \times 10^{23}$	CUPID-0 [149]	361	$(2.72-5.30)$	$<(1.8-3.5) \times 10^{-5}$
^{100}Mo	$>4.4 \times 10^{22}$	NEMO-3 [167]	598	$(3.84-6.59)$	$<(1.8-3.1) \times 10^{-5}$
^{116}Cd	$>8.2 \times 10^{21}$	Aurora [36]	569	$(3.105-5.43)$	$<(5.3-9.2) \times 10^{-5}$
^{116}Cd	$>8.5 \times 10^{21}$	NEMO-3 [168]	569	$(3.105-5.43)$	$<(5.2-9.0) \times 10^{-5}$
^{136}Xe	$>2.6 \times 10^{24}$	KamLAND-Zen [172]	409	$(1.11-4.77)$	$<(0.4-1.7) \times 10^{-5}$
^{136}Xe	$>4.3 \times 10^{24}$	EXO-200 [157]	409	$(1.11-4.77)$	$<(0.3-1.3) \times 10^{-5}$
^{150}Nd	$>0.3 \times 10^{22}$	NEMO-3 [168]	3100	$(1.707-5.46)$	$<(3.7-12) \times 10^{-5}$
J$\beta\beta(n=2)$					
^{76}Ge	$>2.9 \times 10^{23}$	GERDA [139]	—	—	—
^{82}Se	$>3.8 \times 10^{22}$	CUPID-0 [149]	—	—	—
^{100}Mo	$>9.9 \times 10^{21}$	NEMO-3 [170]	—	—	—
^{116}Cd	$>4.1 \times 10^{21}$	Aurora [36]	—	—	—
^{136}Xe	$>1.0 \times 10^{24}$	KamLAND-Zen [172]	—	—	—
^{136}Xe	$>9.8 \times 10^{23}$	EXO-200 [157]	—	—	—
J$\beta\beta(n=3)$					
^{76}Ge	$>1.2 \times 10^{23}$	GERDA [139]	0.073	0.381	$<1.7 \times 10^{-2}$
^{82}Se	$>1.4 \times 10^{22}$	CUPID-0 [149]	1.22	0.305	$<1.5 \times 10^{-2}$
^{100}Mo	$>4.4 \times 10^{21}$	NEMO-3 [170]	2.42	0.263	$<2.3 \times 10^{-2}$
^{116}Cd	$>2.6 \times 10^{21}$	Aurora [36]	2.28	0.144	$<5.6 \times 10^{-2}$
^{136}Xe	$>4.5 \times 10^{23}$	KamLAND-Zen [172]	1.47	0.160	$<0.47 \times 10^{-2}$
^{136}Xe	$>6.3 \times 10^{23}$	EXO-200 [157]	1.47	0.160	$<0.40 \times 10^{-2}$
JJ$\beta\beta(n=3)$					
^{76}Ge	$>1.2 \times 10^{23}$	GERDA [139]	0.22	0.0026	<1.21

Table 3. (Continued.)

Decay/Isotope	$T_{1/2}$ (yr)	Experiment	G (10^{-18} yr^{-1})	NME	g_J
^{82}Se	$>1.4 \times 10^{22}$	CUPID-0 [149]	3.54	0.0020	<1.18
^{100}Mo	$>4.4 \times 10^{21}$	NEMO-3 [170]	6.15	0.0019	<1.41
^{116}Cd	$>2.6 \times 10^{21}$	Aurora [36]	5.23	0.000 945	<2.37
^{136}Xe	$>4.5 \times 10^{23}$	KamLAND-Zen [172]	3.05	0.0011	<0.69
^{136}Xe	$>6.3 \times 10^{23}$	EXO-200 [157]	3.05	0.0011	<0.64
JJ$\beta\beta(n=7)$					
^{76}Ge	$>1.0 \times 10^{23}$	GERDA [139]	0.42	0.0026	<1.08
^{82}Se	$>2.2 \times 10^{21}$	CUPID-0 [149]	26.9	0.0020	<1.13
^{100}Mo	$>1.2 \times 10^{21}$	NEMO-3 [170]	50.8	0.0019	<1.41
^{116}Cd	$>8.9 \times 10^{20}$	Aurora [36]	33.9	0.000 945	<2.37
^{136}Xe	$>1.1 \times 10^{22}$	KamLAND-Zen [172]	12.5	0.0011	<1.23
^{136}Xe	$>5.1 \times 10^{22}$	EXO-200 [157]	12.5	0.0011	<0.84
$\phi\beta\beta(\epsilon_{RR})$					
^{136}Xe	$>3.7 \times 10^{24}$	EXO-200 [157]	—	—	—
$\phi\beta\beta(\epsilon_{RL})$					
^{136}Xe	$>4.1 \times 10^{24}$	EXO-200 [157]	—	—	—

competitive sensitivities can be achieved even with the relatively lower-statistics event samples that will be collected by forthcoming demonstrator experiments, such as the SuperNEMO Demonstrator (see section 5.5) or NEXT-100 (see section 5.3), or their successors (i.e. SuperNEMO and NEXT-HD). Unfortunately, at this moment in time, the performance of these future detectors is not specified at the level needed to run precise sensitivity studies, so we will summarise here only the general idea of these alternative searches.

In general, the single-electron energy distribution can be derived from the phase space in equation (5), similarly to what we have discussed for the two-electron summed energy distribution:

$$\frac{\mathrm{d}\Gamma^{2\nu}}{\mathrm{d}E_{e1}} = |\mathcal{M}^{2\nu}|^2 \frac{\mathrm{d}\mathcal{G}^{2\nu}}{\mathrm{d}E_{e1}} \tag{39}$$

while the angular distribution is given by [109]:

$$\frac{\mathrm{d}\Gamma^{2\nu}}{\mathrm{d}\cos\theta} = \frac{\Gamma^{2\nu}}{2}(1 + K^{2\nu}\cos\theta), \tag{40}$$

where θ is the opening angle between the two electrons and $K^{2\nu}$ the angular correlation factor, whose values are isotope dependent and can be calculated as discussed in [128].

In a SM $2\nu\beta\beta$ decay, the shape of a single electron energy resembles that of a single beta decay, and the electrons are preferably emitted back-to-back to preserve the angular momentum. Even if some angular correlations are present due to the nuclear aspect of the decay, the coefficient $K^{2\nu}$ is negative. Processes beyond the SM $2\nu\beta\beta$ decay can alter both observables in a variety of ways, out of which the most striking case is when right-handed currents force the electrons to be emitted in the same direction to preserve angular momentum [109], resulting in positive values of $K^{2\nu}$. In general, there are many scenarios in which the study of the electron angular distribution would be the most striking signature of new physics in double-β decay [53, 71, 82, 109, 125, 127, 128].

Searches for new physics based on deviations of the single-electron energy distribution would be carried out similarly to what we described in the previous sections for the summed electron energy distributions. The same statistical methods for signal extraction discussed above apply with similar conclusions on the experimental sensitivity and systematic uncertainties. Differently, searches based on deviations of the electron angular distribution will require a totally new approach, for which the primary observable becomes the forward-backward asymmetry of the emitted electrons. The asymmetry $A_\theta^{2\nu}$ is related to the angular correlation coefficient $K^{2\nu}$ through the relation [109]:

$$A_\theta^{2\nu} = \frac{N_{\theta>\pi/2} - N_{\theta<\pi/2}}{N_{\theta>\pi/2} + N_{\theta<\pi/2}} = \frac{1}{2}K^{2\nu}, \tag{41}$$

where $N_{\theta>\pi/2}$ is the number of electrons observed being emitted with relative angle $\theta > \pi/2$, and vice versa. Thus, the asymmetry is simply related to the angular correlation factor, and it is clearly independent of the overall $2\nu\beta\beta$ decay rate.

The discovery power of future-experiment sensitivity to the full decay kinematic can thus be enormous, and it will be ultimately limited by the precision with which the single electron momentum can be measured and by the overall detection efficiency. We anticipate that once results from the next round of demonstrator detectors will inform the design and performance estimation of the successor full-scale experiments, more precise studies of these exciting discovery opportunities will rapidly become available.

5. Double-β decay experiments and constraints

The 80-year-long history of double-β decay experiments has seen a variety of technologies and concepts being tested and developed over the years with the standing goal of reducing backgrounds and increasing the isotope mass. A pivotal time for the field was around the turn of the century when the unexpected discovery that neutrinos are massive [129] raised the question of whether that mass could be due to the peculiar mechanism conceived by Majorana [130–132], a hypothesis that can be proven by observing $0\nu\beta\beta$ decay [133]. This boosted the interest for double-β decay experiments, setting in motion a process eventually culminating in the consolidation of five main detection technologies: high-purity germanium semiconductor detectors, cryogenic calorimeters, time projection chambers, large liquid scintillators, and tracking calorimeters. The following sections review the most recent experiments related to these technologies and the community's plan for the next-generation projects. We conclude with a summary of the state-of-the-art constraints on the search for BSM double-β decay in section 5.7 and prospects in section 6.

5.1. HPGe semiconductor detectors

High-Purity Ge (HPGe) detectors have been a leading technology for double-β experiments since the very first $0\nu\beta\beta$ decay searches [134, 135]. HPGe detectors are semiconductor devices in which electron-hole charge carriers produced by ionization processes are collected by an electric field applied throughout an ultra-pure Ge crystal isotopically enriched in ^{76}Ge up to 92%. The typical detector size is 1–3 kg, requiring the simultaneous operation of multiple detectors to reach a large target mass. HPGe detectors have superior energy resolution, the best of any double-β decay experiment, while also providing information on the event topology. The two electrons emitted in double-β decays produce a very localized energy deposition within $\sim 1 \, \mathrm{mm}^3$ in germanium. Therefore, double-β decays are fully contained within the active detector region, leading to very high detection efficiency.

The most sensitive double-β decay searches based on HPGe detectors have been conducted by the Germanium Detector Array (GERDA) experiment [136] and the MAJORANA DEMONSTRATOR [137]. GERDA was located at the Laboratori Nazionali del Gran Sasso (LNGS) in central Italy and operated about 40 kg of HPGe detectors directly immersed in a LAr volume instrumented to detect its scintillation light. The MAJORANA DEMONSTRATOR was located in the Sanford Underground Research Facility (SURF) in South Dakota and operated about 30 kg of HPGe detectors in two vacuum cryostats. The results of the GERDA and MAJORANA DEMONSTRATOR experiments have demonstrated the feasibility of building a ton-scale ^{76}Ge-based $0\nu\beta\beta$ decay experiment with an ultra-low background and superior energy resolution. With the GERDA and MAJORANA DEMONSTRATOR experiments now completed, the next generation experiment will be realized in the framework of the LEGEND project, following two stages named LEGEND-200 and LEGEND-1000 [138]. LEGEND-200 has just started approaching physics data taking with 200 kg of HPGe detectors in the upgraded GERDA infrastructure. LEGEND-1000 is currently under preparation and is expected to come online towards the end of the decade.

The GERDA experiment has performed several searches for BSM double-β decays of ^{76}Ge in [139]. Its most sensitive search for Majorons-mediated decays led to half-life constraints of 6.4×10^{23} years, 2.9×10^{23} years, 1.2×10^{23} years, and 1.0×10^{23} years (at 90% C.L.), for the decays with spectral index $n = 1$, 2, 3, and 7, respectively. In the same work, limits on Lorentz violation and the decay into light exotic fermions have also been derived. The Lorentz violating isotropic coefficient $\mathring{a}_{of}^{(3)}$ has been constrained to $(-2.7 < \mathring{a}_{of}^{(3)} < 6.2) \cdot 10^{-6}$ GeV at

90% C.L. In the search for double-β decays into sterile neutrinos, the most stringent limit was obtained for masses between 500 and 600 keV. For these masses, the 90% C.L. interval obtained on the mixing between sterile and active neutrinos is $\sin^2\theta < 0.013$. In the search for double-β decays into Z_2-odd fermions, limits on the decay half-life have been derived in the range $(0.18-2.5) \times 10^{23}$ years, at 90% C.L. The best limit of 2.5×10^{23} years was obtained for a mass of 400 keV and corresponds to a limit on the coupling constant $g_\chi < (0.6 - 1.4) \times 10^{-3}$ MeV^{-2}, where the range is due to the NME uncertainties.

5.2. Cryogenic calorimeters

Cryogenic calorimeters, which are also referred to as bolometers, have been employed for $0\nu\beta\beta$ decay and dark matter searches since the 80 s [140–142]. A bolometer essentially consists of an energy absorber, in which the energy of an interacting particle is deposited, and a phonon sensor, which converts this energy, i.e. the phonons, into a measurable signal. Typically, semiconductor thermistors are used as phonon sensors in double-β decay experiments. They rely on the change in resistance of the semiconductor materials, which requires the bolometers to be operated at temperatures of around 10 or a few tens of mK.

The cryogenic calorimeters are extremely versatile tools, as the crystal material can be chosen in order to study a variety of double-β decay isotopes. In addition, materials with scintillation properties can be used, allowing the simultaneous measurement of heat and light signals, enabling particle identification [143]. Further advantages of this detection technique are an excellent energy resolution and very high detection efficiency. The limited crystal dimensions (typically between 0.2 and 0.8 kg) require the operation of thousands of cryogenic calorimeters to reach target masses of hundreds of kilograms or larger. This poses challenging requirements to the cryogenic infrastructure that needs to keep a ton of material stably at mK temperatures for years.

Currently, the largest bolometric experiment is the Cryogenic Underground Observatory for Rare Events (CUORE) at LNGS, which operates about 750 kg of TeO$_2$ crystals with natural isotopic composition (corresponding to 206 kg of ^{130}Te) in a large cryogen-free cryostat [144]. The CUORE experiment successfully demonstrated the feasibility of a ton-scale bolometric experiment [145], leading to CUPID, the next generation bolometric experiment CUORE Upgrade with Particle Identification enabled by the usage of scintillating bolometers. As part of the R&D towards CUPID, two independent experiments have produced constraints on BSM physics. The first one is CUPID-0, at LNGS, which utilized ZnSe crystals enriched in ^{82}Se [146]. The second one is CUPID-Mo at LSM in France, which utilized Li$_2$MoO$_4$ crystals enriched in ^{100}Mo [147].

The CUPID-0 experiment searched for Lorentz violating double-β decay of ^{82}Se [148] and for double-β decays with the emission of Majorons [149]. In the first work, the Lorentz violating coefficient $\mathring{a}_{of}^{(3)}$ has been constrained to $<4.1 \times 10^{-6}$ GeV at 90% C.I. In the second work, limits on the half-life of the decays involving Majorons have been derived. These are 1.2×10^{23} years, 3.8×10^{22} years, 1.4×10^{22} years, and 2.2×10^{21} years (at 90% C.I.), respectively for the decays with spectral index $n = 1$, 2, 3, and 7.

5.3. Time projection chambers

The first direct observation of $2\nu\beta\beta$ decay in 1987 was made using a Time Projection Chamber (TPC) [5]. Since then, this technology has been at the forefront of $0\nu\beta\beta$ decay searches because of the combination of mass scalability and optimal background discrimination capabilities enabled by the 3D reconstruction of the event topology, position, and energy. TPCs are particularly well-suited to search for $0\nu\beta\beta$ decay of ^{136}Xe: Xe is a noble

element that can be used directly in TPCs as a liquid or gas. On the other hand, TPC detectors have a limited energy resolution and require a multivariate analysis to constrain background features close to the $Q_{\beta\beta}$, which are often not resolved (e.g. ^{214}Bi γ line at 2447.7 keV, just below the ^{136}Xe $Q_{\beta\beta}$).

The most sensitive liquid-Xe TPC among the current generation of double-β decay experiments was EXO-200 at WIPP near Carlsbad New Mexico. EXO-200 was a single-phase liquid-Xe TPC, filled with 161 kg of ^{136}Xe [150]. EXO-200 demonstrated the capabilities of a monolithic liquid-Xe TPC, which includes relatively good energy resolution, near-maximal signal detection efficiency, and solid topological discrimination of backgrounds [151]. Building on it, the next generation ton-scale ^{136}Xe-based $0\nu\beta\beta$ decay experiment nEXO is currently being proposed [152].

High-pressure gaseous Xe TPCs for $2\nu\beta\beta$-decay have been developed in the context of the NEXT project [153]. The gaseous Xe TPCs with electroluminescent read-out feature a better energy resolution compared to liquid-Xe TPCs, and the potential of reconstructing charged particle tracks and extracting additional information on the kinematic of double-β decay events [154]. As the final goal, the NEXT collaboration envisions a ton-scale phase operating a full ton of ^{136}Xe in the form of enriched Xe gas [155] and possibly deploying technologies for the identification of the ^{136}Xe decay daughter isotope [156].

The EXO-200 experiment has searched for BSM double-β decays of ^{136}Xe. It sets upper limits on Majorons emitting decays at the level of 4.3×10^{24} years, 1.5×10^{24} years, 6.3×10^{23} years, and 5.1×10^{22} years (at 90% C.L.), respectively for the decays with spectral index $n = 1$, 2, 3, and 7 [157]. In the same work, limits on the emission of a Majoron-like particle via non-standard RH interactions have also been derived. The half-life of these decays has been constrained at 90% C.L. to 3.7×10^{24} years and 4.1×10^{24} years, respectively, for right-handed and left-handed quark currents. The EXO-200 experiment first searched for Lorentz violation in $2\nu\beta\beta$ decay [158]. The Lorentz violating coefficient $\mathring{a}_{of}^{(3)}$ was constrained to $-2.65 \times 10^{-5}\,\text{GeV} < \mathring{a}_{of}^{(3)} < 7.60 \times 10^{-6}\,\text{GeV}$ at 90% C.L.

5.4. Large liquid scintillators

Large liquid scintillator detectors have historically been the most mass-scalable technology used by $0\nu\beta\beta$ experiments. The scintillator can be doped with different isotopes of interest for these searches, including ^{136}Xe and ^{130}Te. Decays occurring within the detector create scintillation photons, which travel straight to the outer surface of the scintillator volume where they are read out by photo-multipliers tubes. The event position and energy release are reconstructed using the time-of-flight of the photons and their number. Multivariate analysis can also provide some information on the initial spatial extension of the energy deposition, giving an extra handle to tag background-like events.

The most important liquid scintillator detector in the field is operated by the KamLAND-Zen experiment in the Kamioka Mine in Japan [159]. It consists of a nylon balloon placed at the center of the detector volume and filled with a liquid scintillator in which ^{136}Xe has been dissolved. After a successful first phase (KamLAND-Zen 400) with up to 340 kg of ^{136}Xe, the second phase (KamLAND-Zen 800) is currently running with about 680 kg of ^{136}Xe [160]. With the first 1.6 years of data, KamLAND-Zen 800 produced a world-leading $0\nu\beta\beta$ decay half-life limit [160]. The KamLAND-Zen collaboration is already preparing for the ton-scale phase (KamLAND2-Zen) in which about 1 ton of ^{136}Xe will be deployed [161].

The technology of large liquid scintillators is largely employed in neutrino experiments. Among future large liquid scintillator experiments, we shall mention the SNO experiment. This is a multi-purpose neutrino experiment located at SNOLAB in Canada containing 780

tons of organic liquid scintillator [162]. A future upgrade of the experiment is planned, in which the liquid scintillator will be loaded with a double-β decaying isotope to search for $0\nu\beta\beta$ decay. The isotope to be used is still under investigation [162].

The KamLAND-Zen experiment searched for double-β decays with the emission of Majorons [163]. Limits on the half-life of these decays have been derived at 90% C.L.: 2.6×10^{24} years, 1.0×10^{24} years, 4.5×10^{23} years, and 1.1×10^{22} years, respectively for the decays with spectral index $n = 1, 2, 3$, and 7.

5.5. Tracking calorimeters

Tracking calorimeters are the only technology capable of measuring with high accuracy the kinematics of electrons emitted in double-β decays, such as the single-electron energy and the electron angular distribution. Measuring these quantities would give precious inputs to pin down the actual channel mediating the $0\nu\beta\beta$ decay [164]. It would also strongly enhance the sensitivity to BSM double-β decays discussed in this review.

The tracking capability is obtained by decoupling the double-β decay isotope from the detector. The target isotope is placed on a thin foil, immersed in a magnetic field, and surrounded by tracking and calorimetric layers. This configuration enables the measurement of the electron momentum through its bending in the magnetic field, and the measure of its energy when it enters the calorimeters. Unfortunately, it reduces the detection efficiency. The requirement of using very thin foils to minimize energy losses makes it extremely challenging to scale up the isotope mass.

The NEMO-3 experiment utilized this technology to search for $0\nu\beta\beta$ decay of several isotopes at the Laboratoire Souterrain de Modane (LSM) in France. Masses from a few grams to a few kilograms of the isotopes of interest were deployed in separate sectors of the detector (6.99 g of ^{48}Ca [39], 0.932 kg of ^{82}Se [165], 9.4 g of ^{96}Zr [166], 6.914 kg of ^{100}Mo [167], 410 g of ^{116}Cd [168], and 36.6 g of ^{150}Nd [30]). A next-generation tracking calorimeter detector is the SuperNEMO Demonstrator, which is based on the technology demonstrated by NEMO-3 [169]. In its first phase, the SuperNEMO Demonstrator will deploy one module with 7 kg of ^{82}Se. A future full-scale experiment is foreseen, consisting of multiple modules aiming for a total ^{82}Se mass of 100 kg.

The NEMO-3 experiment searched for Majoron-involving double-β decays in several isotopes: ^{100}Mo [167, 170], ^{82}Se [165], ^{116}Cd [168], ^{48}Ca [39], and ^{150}Nd [30]. Limits on the half-life of the decay corresponding to spectral index $n = 1$ have been derived (at 90% C.L.) for all the used isotopes: 4.6×10^{21} years with ^{48}Ca, 3.7×10^{22} years with ^{82}Se, 4.4×10^{22} years with ^{100}Mo, 8.5×10^{21} yr with ^{116}Cd, and 0.3×10^{22} years with ^{150}Nd. Limits on the half-life of the decays corresponding to spectral indexes $n = 2, 3$, and 7 have been derived only with ^{100}Mo, because of the lower-statistics data sets and the higher background achieved with the other isotopes. The corresponding limits at 90% C.L. are: 9.9×10^{21} years, 4.4×10^{21} years and 1.2×10^{21} years, respectively for the $n = 2, 3$, and 7. The NEMO-3 experiment also searched for Lorentz violation in the $2\nu\beta\beta$ decay of ^{100}Mo and the ^{100}Mo $2\nu\beta\beta$ decay with bosonic neutrinos [170]. The Lorentz violating isotropic coefficient $\mathring{a}_{of}^{(3)}$ has been constrained to $(-4.2 < \mathring{a}_{of}^{(3)} < 3.5) \cdot 10^{-7}$ GeV at 90% C.L. The half-life of the ^{100}Mo $2\nu\beta\beta$ decay with bosonic neutrinos was constrained to 1.2×10^{21} years, which corresponds to an upper limit on the bosonic neutrino contribution of $\sin \chi < 0.27$ at 90% C.L.

5.6. Other technologies

We should mention the Aurora experiment at LNGS among the experiments using technologies other than those described in the previous subsections. It utilized more than 1 kg of radio-pure cadmium tungstate (^{116}CdWO$_4$) scintillating crystals enriched in the ^{116}Cd isotope [171]. Even if this technology is not competitive in terms of $0\nu\beta\beta$ decay sensitivities and there is no concrete plan to scale it to a ton-scale $0\nu\beta\beta$ decay experiments, the Aurora experiment has produced competitive constraints in the search for BSM double-β decays of ^{116}Cd [36]. They set limits on the half-life of Majorons emitting decays with the emission of Majorons at the order of 10^{21} years, while the most stringent limit was obtained for the $n = 1$ spectral index: $T_{1/2} > 8.2 \times 10^{21}$ years (at 90% C.L.). In the same work, they searched for Lorentz violation and obtained a limit on the isotropic coefficient of $\mathring{a}_{of}^{(3)} < 4.0 \cdot 10^{-6}$ GeV (at 90% C.L.).

5.7. Most sensitive constraints

In this section we summarise the most sensitive constraints reported by all experiments mentioned in the previous sections, grouping them based on the new physics searched.

Double-β decay with the emission of Majorons. A summary of the latest results obtained by different double-β decay experiments is presented in table 3. The most stringent limits, regardless of the isotope and the experiment, are obtained for the model corresponding to a spectral index $n = 1$. In fact, the energy distribution predicted for this decay differs the most from the SM $2\nu\beta\beta$ decay compared to other spectral indexes, as shown in figure 5. Among different experiments, the best limit on the half-life of the J$\beta\beta$ decay ($n = 1$ mode) is obtained by the EXO-200 experiment with ^{136}Xe: 4.3×10^{24} years at 90% C.L. EXO-200 also obtained the best limits on the half-life of the J$\beta\beta$/JJ$\beta\beta$ decays ($n = 3$ modes): 6.3×10^{23} years. For the J$\beta\beta$ decay ($n = 2$ mode), the KamLAND-Zen experiment set the most competitive limit on the half-life at 1.0×10^{24} years, while the GERDA experiment set the most competitive limit on the half-life of the JJ$\beta\beta$ decay ($n = 7$ mode): 1.0×10^{23} years. Recently, EXO-200 has searched for BSM double-β decays in which a Majoron-like particle is emitted via non-standard right-handed currents were also investigated [157]. Limits were derived on such a decay for both right-handed and left-handed hadronic currents: 3.7×10^{24} years and 4.1×10^{24} years, respectively.

Lorentz-violating $2\nu\beta\beta$ decay. A summary of the latest results obtained by different double-β decay experiments is presented in table 4. The most stringent limit on $\mathring{a}_{of}^{(3)}$ comes from NEMO-3 and is at the order of 10^{-7}, a factor 10 better than all the other experiments. This result is attributed to the much larger statistics of $2\nu\beta\beta$ decay events achieved by the NEMO-3 experiment ($\sim 1.9 \times 10^5$ events in the analysis range). However, part of this difference comes from the statistical treatments as only the CUPID-0 and GERDA experiments used the approach highlighted in this review for class III models (see section 4), to which the Lorentz violating $2\nu\beta\beta$ decay belongs. Aurora, NEMO-3, and EXO-200 treated the perturbation introduced by Lorentz violation as an independent component in the fit, neglecting any correlation with the SM $2\nu\beta\beta$ decay distribution in the result. Nevertheless, the impact is hard to quantify and goes beyond the scope of this work. When comparing different results, it should also be considered that the limits on $\mathring{a}_{of}^{(3)}$ depend on the calculated phase space ratio between the SM $2\nu\beta\beta$ decay and the LV perturbation. The different experiments reviewed in table 4 used different calculations. In recent work, improved phase space calculations were performed, in which the Fermi functions are built with exact electron wave functions obtained by numerically solving a Dirac equation in a realistic Coulomb-type potential, including finite nuclear size and screening effects [173]. Differences up to 30% for heavier nuclei were found

Table 4. Summary of the results obtained by different double-β decay experiments in the search for Lorentz violation.

Isotope	$\mathring{a}_{of}^{(3)}$(GeV)	Experiment
^{76}Ge	$(-2.7 < \mathring{a}_{of}^{(3)} < 6.2) \times 10^{-6}$	GERDA [139]
^{82}Se	$\mathring{a}_{of}^{(3)} < 4.1 \times 10^{-6}$	CUPID-0 [148]
^{100}Mo	$(-4.2 < \mathring{a}_{of}^{(3)} < 3.5) \times 10^{-7}$	NEMO-3 [170]
^{116}Cd	$\mathring{a}_{of}^{(3)} < 4.0 \times 10^{-6}$	Aurora [36]
^{136}Xe	$-2.65 \times 10^{-5} < \mathring{a}_{of}^{(3)} < 7.6 \times 10^{-6}$	EXO-200 [158]

between these improved calculations and the previous calculations using approximated analytical Fermi functions. As pointed out in [173], for example, there is a relevant difference between the newly calculated phase space ratio and the one used by the CUPID-0 collaboration in [148].

$2\nu\beta\beta$ decay with bosonic neutrinos. The experimental search for an admixture of bosonic and fermionic neutrinos through the search for distortions of the $2\nu\beta\beta$ decay spectrum has been performed only by the NEMO-3 experiment with ^{100}Mo [170]. They obtained an upper limit on the bosonic neutrino contribution $\sin^2 \chi < 0.27$ at 90% C.L. Also in this case, the statistical treatment does not follow the receipt given in 4 for class II models as it neglects the correlation between the SM $2\nu\beta\beta$ decay (fermionic neutrinos) and $2\nu\beta\beta$ decay with bosonic neutrinos distributions. As already introduced in 3.2.2, searches with other isotopes than ^{100}Mo might be disfavoured by the small predicted ratio r_0 with which the fermionic and bosonic contributions are weighted in the total $2\nu\beta\beta$ decay rate.

Double-β decay into sterile neutrinos and Z_2-odd fermions. The experimental search for light exotic fermions, i.e. sterile neutrinos and Z_2-odd fermions, has been performed only by the GERDA experiment with ^{76}Ge [139], which set a limit on the mixing between active and sterile neutrinos $\sin^2 \theta < 0.013$ for a sterile neutrino mass of $m_N = 500$ keV. The limits get worse for lower and higher masses ($\sin^2 \theta < 0.15$ for $m_N = 100$ keV, $\sin^2 \theta < 0.050$ for $m_N = 900$ keV). GERDA has also set the first direct experimental constraints on the emission of two Z_2-odd fermions, constraining the half-life of the corresponding decay to 2.5×10^{23} years for a mass $m_\chi = 400$ keV, which translates into a constraint on the coupling g_χ of $(0.6-1.4) \times 10^{-3}$ MeV^{-2}. Again, limits get worse for smaller and larger masses.

6. Outlook and prospects

Hunting for the extremely rare $0\nu\beta\beta$ decay, existing experiments collected up to millions of $2\nu\beta\beta$ decay events. These statistics are expected to increase rapidly as future experiments, with a much larger target mass, will start taking data. We showed in this review that $2\nu\beta\beta$ decays could be used as probes of new physics.

Since the first experimental searches for double-β decay with the emission of one or two Majorons, we have seen remarkable progress both in the theoretical description of the decays and in the experimental technologies. Improved and more precise calculations of the phase space factors and NMEs are available today, which are essential to convert the experimental constraints on the half-life of the decays into a coupling between the exotic particle, i.e. the Majoron, and neutrinos. On the other hand, the experiments reached incredible precision in the study of $2\nu\beta\beta$ decay with large statistics data samples and drastic reduction of the background compared to their

predecessors, pushing the bounds on the half-life of these decays up to 10^{24} years. Limits on the neutrino-Majoron coupling g_J for the Majoron model leading to $n = 1$ are also available from astrophysics. Supernova observations allow excluding the region of the parameter space $4 \times 10^{-7} < g_J < 2 \times 10^{-5}$ by studying the role of Majorons in the Supernova explosion [174, 175]. Current double-β decay experiments completely excluded the region above the lower Supernova bound. The combined results bring the upper bound down to $g_J < 4 \times 10^{-7}$, far from the sensitivity of any future double-β decay experiment. Nevertheless, one should remember that Supernova bounds are model-dependent and rely upon additional assumptions. To date, double-β decays provide the best direct constraints on the neutrino-Majoron coupling.

Light exotic fermions can also be searched in double-β decays. Depending on the $Q_{\beta\beta}$ of the double-β decay isotope, one or two exotic fermions with a mass between a few hundred keV and a few MeV can be emitted in double-β decay. In the search for sterile neutrinos in this mass range, current double-β decay experiments provide bounds that are still weaker than the existing single-β decay bounds, as predicted in [82, 83] and confirmed by GERDA results [139]. Still, future experiments could reach unexplored regions of the parameter space, down to $\sin^2\theta \sim 10^{-3} - 10^{-4}$, for masses between 100 and 2000 keV. To date, no experiment exists or is planned with the capability of testing this part of the parameter space ($100 \, \text{keV} < m_N < 2000 \, \text{keV}$).[9] Therefore, future double-β decay experiments will provide the best direct constraints on the active-sterile neutrino mixing in the aforementioned mass range. In addition, double-β decay experiments offer a unique opportunity to test all those models in which only the double production of light exotic fermions is allowed, leading to the best direct constraints on the coupling between these exotic fermions and neutrinos of the order of $g_\chi \sim 10^{-4} \, \text{MeV}^{-2}$.

Studying the $2\nu\beta\beta$ decay spectrum can provide a sensitive test of Lorentz violation. Current experiments constrained the Lorentz-violating coefficient $\mathring{a}_{of}^{(3)}$ at the level of $|\mathring{a}_{of}^{(3)}| < 10^{-6} - 10^{-7} \, \text{GeV}$. The study of the single-β decay spectrum also provides a sensitive constraint to the same coefficient $\mathring{a}_{of}^{(3)}$. In [93], a constraint on $\mathring{a}_{of}^{(3)}$ was derived using tritium β decay data from the Mainz and Troitsk experiments: $|\mathring{a}_{of}^{(3)}| < 2.0 \times 10^{-8} \, \text{GeV}$, which is already more competitive of the constraints from double-β decays. Recently, the KATRIN experiment performed a similar analysis using a small set of available data, setting a limit at $|\mathring{a}_{of}^{(3)}| < 3.0 \times 10^{-8} \, \text{GeV}$ [176]. This limit is expected to further improve up to a sensitivity of $10^{-9} \, \text{GeV}$ or more with the full KATRIN exposure [95]. Future double-β decay experiments will be able to improve their current limits (in the best case scenario by a factor of $\sqrt{1/\mathcal{E}}$), nevertheless, hardly reaching single-β decay experiments sensitivity.

A purely bosonic neutrino would substantially change the total double-β decay rate, therefore, the measured $2\nu\beta\beta$ decay half-life values. Several precision measurements of the $2\nu\beta\beta$ decay half-life of different isotopes completely ruled out the hypothesis of a purely bosonic neutrino. On the other hand, experimental data does not completely exclude the hypothesis of a mixed statistic with a partly bosonic neutrino. The only experimental upper limit on the admixture of the bosonic component was set by the NEMO-3 experiment with ^{100}Mo. The sensitivity to spectral distortions depends on the ratio r_0 between the rates for purely bosonic and purely fermionic neutrinos, which involves phase space factors and NMEs of the two decays. Consequently, some isotopes are favored (i.e. ^{100}Mo) for future searches of bosonic neutrino admixture compared to others (i.e. ^{76}Ge), for which the very small value of r_0 neutralizes possible effects induced by a partly bosonic neutrino.

---

[9] See figure 7 in [81].

Finally, $2\nu\beta\beta$ decays can be used as a probe of hidden non-standard interaction of neutrinos, like strong neutrino self-interactions and the presence of right-handed currents in weak interactions. Although it was shown that already current experiments could be competitive in constraining such non-standard operators [109, 125], no experimental searches have been performed yet.

Acknowledgments

Data availability statement

There are no new data in the published manuscript. The data that support the findings of this study are available upon reasonable request from the authors.

ORCID iDs

Elisabetta Bossio ⬛ https://orcid.org/0000-0001-9304-1829
Matteo Agostini ⬛ https://orcid.org/0000-0003-1151-5301

References

[1] Detwiler J A and Robertson R G H 2023 *Phys. Rev.*C **107** L042501
[2] Alanssari M *et al* 2016 *Phys. Rev. Lett.* **116** 072501
[3] Goeppert-Mayer M 1935 *Phys. Rev.* **48** 512–6
[4] Inghram M G and Reynolds J H 1950 *Phys. Rev.* **78** 822–3
[5] Elliott S R, Hahn A A and Moe M K 1987 *Phys. Rev. Lett.* **59** 2020–3
[6] Barabash A S 2020 *Universe* **6** 159
[7] Agostini M, Benato G, Detwiler J A, Menéndez J and Vissani F 2023 *Rev. Mod. Phys.* **95** 025002
[8] Barabash A S 2011 *Phys. Atom. Nucl.* **74** 603–13
[9] Saakyan R 2013 *Ann. Rev. Nucl. Part. Sci.* **63** 503–29
[10] Takaoka N and Ogata K 1966 *Z. Naturforsch.*A **21** 84–90
[11] Kirsten T, Gentner W and Schaeffer O A 1967 *Z. Phys.* **202** 273–92
[12] Hennecke E W, Manuel O K and Sabu D D 1975 *Phys. Rev.*C **11** 1378–84
[13] Doi M, Kotani T and Takasugi E 1985 *Prog. Theor. Phys. Suppl.* **83** 1–175
[14] Vasenko A A, Kirpichnikov I V, Kuznetsov V A, Starostin A S, Djanyan A G, Pogosov V S, Shachysisyan S P and Tamanyan A G 1990 *Mod. Phys. Lett.*A **05** 1299–306
[15] Ejiri H *et al* 1991 *Phys. Lett.*B **258** 17–23
[16] Elliott S R, Moe M K, Nelson M A and Vient M A 1991 *J. Phys. G: Nucl. Part. Phys.* **17** S145
[17] De Silva A, Moe M K, Nelson M A and Vient M A 1997 *Phys. Rev.*C **56** 2451–67
[18] Dassié D *et al* 1995 *Phys. Rev.*D **51** 2090–100
[19] Elliott S R, Hahn A A, Moe M K, Nelson M A and Vient M A 1992 *Phys. Rev.*C **46** 1535–7
[20] Arnold R *et al* 1998 *Nucl. Phys.*A **636** 209–23
[21] Ejiri H *et al* 1995 *J. Phys. Soc. Jpn.* **64** 339–43
[22] Arnold R *et al* (NEMO) 1995 *JETP Lett.* **61** 170–4 https://hal.in2p3.fr/in2p3-00015147

[23] Danevich F A, Georgadze A S, Kobychev V V, Kropivyansky B N, Kuts V N, Nikolaiko A S, Tretyak V I and Zdesenko Y 1995 *Phys. Lett.*B **344** 72–8
[24] Collaboration N *et al* 1996 *Z. Phys.* C **72** 239–47
[25] Balysh A, De Silva A, Lebedev V I, Lou K, Moe M K, Nelson M A, Piepke A, Pronskiy A, Vient M A and Vogel P 1996 *Phys. Rev. Lett.* **77** 5186–9
[26] Arnold R *et al* 1999 *Nucl. Phys.*A **658** 299–312
[27] Turkevich A L, Economou T E and Cowan G A 1991 *Phys. Rev. Lett.* **67** 3211–4
[28] Barabash A S, Brudanin V B and Collaboration N 2011 *Phys. At. Nucl.* **74** 312–7
[29] Ackerman N *et al* (EXO-200) 2011 *Phys. Rev. Lett.* **107** 212501
[30] Arnold R *et al* (NEMO-3) 2016 *Phys. Rev.* D **94** 072003
[31] Bossio E 2022 Beyond the Standard Model physics searches with double-beta decays *PhD thesis Munich* Tech. Univ.
[32] Agostini M *et al* (GERDA) 2023 *Phys. Rev. Lett.* **131** 142501
[33] Azzolini O *et al* 2019 *Phys. Rev. Lett.* **123** 262501
[34] Argyriades J *et al* (NEMO-3) 2010 *Nucl. Phys.* A **847** 168–79
[35] Armengaud E *et al* 2020 *Eur. Phys. J.* C **80** 674
[36] Barabash A S *et al* 2018 *Phys. Rev.*D **98** 092007
[37] Adams D Q *et al* (CUORE) 2021 *Phys. Rev. Lett.* **126** 171801
[38] Albert J B *et al* (EXO-200) 2014 *Phys. Rev.* C **89** 015502
[39] Arnold R *et al* (NEMO-3) 2016 *Phys. Rev.* D **93** 112008
[40] Tretyak V I and Zdesenko Y G 2002 *At. Data Nucl. Data Tables* **80** 83–116
[41] Doi M, Kotani T, Nishiura H, Okuda K and Takasugi E 1981 *Prog. Theor. Phys.* **66** 1739–64
   Doi M, Kotani T, Nishiura H, Okuda K and Takasugi E 1982 *Prog. Theor. Phys.* **68** 347
[42] Doi M, Kotani T, Nishiura H and Takasugi E 1983 *Prog. Theor. Phys.* **69** 602–35
[43] Tomoda T 1991 *Rep. Prog. Phys.* **54** 53
[44] Kotila J and Iachello F 2012 *Phys. Rev.*C **85** 034316
[45] Aker M *et al* (KATRIN) 2022 *Nat. Phys.* **18** 160–6
[46] Abbott T M C *et al* (DES) 2022 *Phys. Rev.*D **105** 023520
[47] Chikashige Y, Mohapatra R N and Peccei R D 1981 *Phys. Lett.*B **98** 265–8
[48] Chikashige Y, Mohapatra R N and Peccei R D 1980 *Phys. Rev. Lett.* **45** 1926–9
[49] Gelmini G B and Roncadelli M 1981 *Phys. Lett.*B **99** 411–5
[50] Santamaria A and Valle J 1987 *Phys. Lett.*B **195** 423–8
[51] Santamaria A and Valle J W F 1988 *Phys. Rev. Lett.* **60** 397–400
[52] Santamaria A and Valle J W F 1989 *Phys. Rev.*D **39** 1780–3
[53] Cepedello R, Deppisch F F, González L, Hati C and Hirsch M 2019 *Phys. Rev. Lett.* **122** 181801
[54] Georgi H M, Glashow S L and Nussinov S 1981 *Nucl. Phys.*B **193** 297–316
[55] Vergados J 1982 *Phys. Lett.*B **109** 96–100
[56] Doi M, Kotani T and Takasugi E 1988 *Phys. Rev.*D **37** 2575–89
[57] Mohapatra R N and Takasugi E 1988 *Phys. Lett.*B **211** 192–6
[58] Steinberger J 1992 *Electroweak Physics Beyond the Standard Model* (World Scientific)
[59] Schael S *et al* (ALEPH, DELPHI, L3, OPAL, and SLD Collaborations, LEP Electroweak Working Group, SLD Electroweak Group, SLD Heavy Flavour Group) 2006 *Phys. Rep.* **427** 257–454
[60] Elliott S R, Hahn A A and Moe M K 1987 *Phys. Rev. Lett.* **59** 1649–51
[61] Avignone F T, Brodzinski R L, Miley H S and Reeves J H 1987 *Phys. Lett.*B **198** 253–4
[62] Fisher P, Boehm F, Henrikson H, Bovet E, Egger J P, Vuilleumier J L and Gabathuler K 1987 *Phys. Lett.*B **192** 460–2
[63] Berezhiani Z G, Smirnov A Y and Valle J W F 1992 *Phys. Lett.*B **291** 99–105
[64] Burgess C P and Cline J M 1993 *Phys. Lett.*B **298** 141–8
[65] Burgess C P and Cline J M 1994 *Phys. Rev.*D **49** 5925–44
[66] Bamert P, Burgess C P and Mohapatra R N 1995 *Nucl. Phys.*B **449** 25–48
[67] Carone C D 1993 *Phys. Lett.*B **308** 85–8
[68] Mohapatra R N, Perez-Lorenzana A and de S Pires C A 2000 *Phys. Lett.*B **491** 143–7
[69] Hirsch M, Klapdor-Kleingrothaus H V, Kovalenko S G and Pas H 1996 *Phys. Lett.*B **372** 8–14
[70] Kotila J, Barea J and Iachello F 2015 *Phys. Rev.*C **91** 064310
   Kotila J, Barea J and Iachello F 2015 *Phys. Rev.*C **92** 029903
[71] Kotila J and Iachello F 2021 *Phys. Rev.*C **103** 044302

[72] Blum K, Nir Y and Shavit M 2018 *Phys. Lett.*B **785** 354–61
[73] Berezinsky V and Valle J W F 1993 *Phys. Lett.*B **318** 360–6
[74] Brune T and Päs H 2019 *Phys. Rev.*D **99** 096005
[75] Dasgupta B and Kopp J 2021 *Phys. Rep.* **928** 1–63
[76] Shrock R E 1980 *Phys. Lett.*B **96** 159–64
[77] Dragoun O and Vénos D 2016 *J. Phys.* **3** 77–113
[78] Riis A S and Hannestad S 2011 *J. Cosmol. Astropart. Phys.* JCAP02(2011)011
[79] Mertens S, Lasserre T, Groh S, Drexlin G, Glueck F, Huber A, Poon A W P, Steidl M, Steinbrink N and Weinheimer C 2015 *J. Cosmol. Astropart. Phys.* JCAP02(2015)020
[80] Abada A, Hernández-Cabezudo A and Marcano X 2019 *J. High Energy Phys.* JHEP01(2019)041
[81] Bolton P D, Deppisch F F and Bhupal Dev P S 2020 *J. High Energy Phys.* JHEP03(2020)170
[82] Bolton P D, Deppisch F F, Gráf L and Šimkovic F 2021 *Phys. Rev.*D **103** 055019
[83] Agostini M, Bossio E, Ibarra A and Marcano X 2021 *Phys. Lett.*B **815** 136127
[84] Kostelecky V A and Samuel S 1989 *Phys. Rev.*D **39** 683–5
[85] Colladay D and Kostelecky V A 1997 *Phys. Rev.*D **55** 6760–74
[86] Colladay D and Kostelecky V A 1998 *Phys. Rev.*D **58** 116002
[87] Kostelecky V A and Tasson J D 2009 *Phys. Rev. Lett.* **102** 010402
[88] Kostelecky A V and Tasson J D 2011 *Phys. Rev.*D **83** 016013
[89] Kostelecky V A and Russell N 2011 *Rev. Mod. Phys.* **83** 11–31
[90] Kostelecky V A and Mewes M 2004 *Phys. Rev.*D **70** 031902
[91] Kostelecky V A and Mewes M 2004 *Phys. Rev.*D **69** 016005
[92] Kostelecky A and Mewes M 2012 *Phys. Rev.*D **85** 096005
[93] Díaz J S, Kostelecký A and Lehnert R 2013 *Phys. Rev.*D **88** 071902
[94] Díaz J S 2014 *Phys. Rev.*D **89** 036002
[95] Lehnert R 2022 *Phys. Lett.*B **828** 137017
[96] Pauli W 1940 *Phys. Rev.* **58** 716–22
[97] Cucurull L, Grifols J A and Toldra R 1996 *Astropart. Phys.* **4** 391–6
[98] Dolgov A D and Smirnov A Y 2005 *Phys. Lett.*B **621** 1–10
[99] Dolgov A D, Hansen S H and Smirnov A Y 2005 *J. Cosmol. Astropart. Phys.* JCAP06(2005)004
[100] de Salas P F, Gariazzo S, Laveder M, Pastor S, Pisanti O and Truong N 2018 *J. Cosmol. Astropart. Phys.* JCAP03(2018)050
[101] Hannestad S, Ringwald A, Tu H and Wong Y Y Y 2005 *J. Cosmol. Astropart. Phys.* JCAP09(2005)014
[102] Brandbyge J and Hannestad S 2017 *J. Cosmol. Astropart. Phys.* JCAP10(2017)015
[103] Iizuka J and Kitabayashi T 2015 *Mod. Phys. Lett.*A **30** 1550003
[104] Choubey S and Kar K 2006 *Phys. Lett.*B **634** 14–22
[105] Barabash A S, Dolgov A D, Dvornicky R, Šimkovic F and Smirnov A Y 2007 *Nucl. Phys.*B **783** 90–111
[106] Ignatiev A Y and Kuzmin V A 2006 *Phys. Lett.*A **359** 26–30
[107] Pati J C and Salam A 1974 *Phys. Rev.*D **10** 275–89
      Pati J C and Salam A 1975 *Phys. Rev.*D **11** 703–703
[108] Bolton P D, Deppisch F F, Hati C, Patra S and Sarkar U 2019 *Phys. Rev.*D **100** 035013
[109] Deppisch F F, Gráf L and Šimkovic F 2020 *Phys. Rev. Lett.* **125** 171801
[110] Deppisch F F, Hirsch M and Pas H 2012 *J. Phys.*G **39** 124007
[111] González-Alonso M, Naviliat-Cuncic O and Severijns N 2019 *Prog. Part. Nucl. Phys.* **104** 165–223
[112] Cirigliano V, Gardner S and Holstein B 2013 *Prog. Part. Nucl. Phys.* **71** 93–118
[113] Greljo A and Marzocca D 2017 *Eur. Phys. J.*C **77** 548
[114] Khachatryan V *et al* (CMS) 2015 *Phys. Rev.*D **91** 092005
[115] Aaboud M *et al* (ATLAS) 2019 *J. High Energy Phys.* JHEP01(2019)016
[116] Riess A G *et al* 2018 *Astrophys. J.* **861** 126
[117] Birrer S *et al* 2019 *Mon. Not. Roy. Astron. Soc.* **484** 4726–53
[118] Aghanim N *et al* (Planck) 2021 *Astron. Astrophys.* **641** A6
      Aghanim N and Planck 2021 *Astron. Astrophys.* **652** C4
[119] Riess A G, Casertano S, Yuan W, Macri L M and Scolnic D 2019 *Astrophys. J.* **876** 85
[120] Oldengott I M, Tram T, Rampf C and Wong Y Y Y 2017 *J. Cosmol. Astropart. Phys.* JCAP11(2017)027
[121] Kreisch C D, Cyr-Racine F and Doré O 2020 *Phys. Rev.*D **101** 123505

[122] Blinov N, Kelly K J, Krnjaic G Z and McDermott S D 2019 *Phys. Rev. Lett.* **123** 191102
[123] Lyu K F, Stamou E and Wang L T 2021 *Phys. Rev.*D **103** 015004
[124] Arcadi G, Heeck J, Heizmann F, Mertens S, Queiroz F S, Rodejohann W, Slezák M and Valerius K 2019 *J. High Energy Phys.* JHEP01(2019)206
[125] Deppisch F F, Gráf L, Rodejohann W and Xu X 2020 *Phys. Rev.*D **102** 051701
[126] Engel J and Menéndez J 2017 *Rep. Prog. Phys.* **80** 046301
[127] Niţescu O V, Ghinescu S A, Mirea M and Stoica S 2021 *Phys. Rev.*D **103** L031701
[128] Niţescu O, Dvornický R, Stoica S and Šimkovic F 2021 *Universe* **7** 147
[129] Fukuda Y *et al* (Super-Kamiokande) 1998 *Phys. Rev. Lett.* **81** 1562–7
[130] Majorana E 1937 *Nuovo Cim.* **14** 171–84
[131] Racah G 1937 *Nuovo Cim.* **14** 322–8
[132] Furry W H 1939 *Phys. Rev.* **56** 1184–93
[133] Schechter J and Valle J W F 1982 *Phys. Rev.*D **25** 2951–4
[134] Fiorini E, Pullia A, Bertolini G, Cappellani F and Restelli G 1967 *Phys. Lett.*B **25** 602–3
[135] Avignone F T and Elliott S R 2019 *Front. Phys.* **7** 6
[136] Agostini M *et al* (GERDA) 2018 *Eur. Phys. J.*C **78** 388
[137] Abgrall N *et al* (Majorana) 2014 *Adv. High Energy Phys.* **2014** 365432
[138] Abgrall N *et al* (LEGEND) 2021 The Large Enriched Germanium Experiment for Neutrinoless ββ Decay *LEGEND-1000 Preconceptual Design Report* arXiv:2107.11462
[139] Agostini M *et al* (GERDA) 2022 *J. Cosmol. Astropart. Phys.* **2022** JCAP12(2022)012
[140] Fiorini E and Niinikoski T O 1984 *Nucl. Instrum. Meth.*A **224** 83–8
[141] Drukier A and Stodolsky L 1984 *Phys. Rev.*D **30** 2295–309
[142] Brofferio C and Dell'Oro S 2018 *Rev. Sci. Instrum.* **89** 121502
[143] Arnaboldi C, Brofferio C, Cremonesi O, Gironi L, Pavan M, Pessina G, Pirro S and Previtali E 2011 *Astropart. Phys.* **34** 797
[144] Alduino C *et al* 2019 *Cryogenics* **102** 9–21
[145] Adams D Q *et al* (CUORE) 2022 *Prog. Part. Nucl. Phys.* **122** 103902
[146] Azzolini O *et al* 2018 *Eur. Phys. J.*C **78** 428
[147] Armengaud E *et al* 2020 *Eur. Phys. J.*C **80** 44
[148] Azzolini O *et al* (CUPID) 2019 *Phys. Rev.*D **100** 092002
[149] Azzolini O *et al* (CUPID-0) 2023 *Phys. Rev.*D **107** 032006
[150] Auger M *et al* 2012 *JINST* **7** P05010
[151] Anton G *et al* (EXO-200) 2019 *Phys. Rev. Lett.* **123** 161802
[152] Adhikari G *et al* 2022 *J. Phys. G: Nucl. Part. Phys.* **49** 015104
[153] Gomez-Cadenas J J, Monrabal Capilla F and Ferrario P 2019 *Front. Phys.* **7** 51
[154] Ferrario P *et al* (NEXT) 2016 *J. High Energy Phys.* JHEP01(2016)104
[155] Adams C *et al* (NEXT) 2021 *J. High Energy Phys.* JHEP08(2021)164
[156] Rivilla I *et al* 2020 *Nature* **583** 48–54
[157] Kharusi S A *et al* (EXO-200) 2021 *Phys. Rev.*D **104** 112002
[158] Albert J B *et al* (EXO-200) 2016 *Phys. Rev.*D **93** 072001
[159] Shirai J and KamLAND-Zen 2017 *J. Phys. Conf. Ser.* **888** 012031
[160] Abe S *et al* (KamLAND-Zen) 2023 *Phys. Rev. Lett.* **130** 051801
[161] Shirai J and KamLAND-Zen 2017 *J. Phys. Conf. Ser.* **888** 012031
[162] Albanese V *et al* (SNO+) 2021 *JINST* **16** P08059
[163] Gando A *et al* (KamLAND-Zen) 2012 *Phys. Rev.*C **86** 021601
[164] Gráf L, Lindner M and Scholer O 2022 *Phys. Rev.*D **106** 035022
[165] Arnold R *et al* (NEMO-3) 2018 *Eur. Phys. J.*C **78** 821
[166] Argyriades J *et al* (NEMO-3) 2010 *Nucl. Phys.*A **847** 168–79
[167] Arnold R *et al* (NEMO-3) 2015 *Phys. Rev.*D **92** 072011
[168] Arnold R *et al* (NEMO-3) 2017 *Phys. Rev.*D **95** 012007
[169] Piquemal F and NEMO 2006 *Phys. Atom. Nucl.* **69** 2096–100
[170] Arnold R *et al* (NEMO-3) 2019 *Eur. Phys. J.*C **79** 440
[171] Barabash A S *et al* 2011 *JINST* **6** P08011
[172] Gando A *et al* (KamLAND-Zen) 2012 *Phys. Rev.*C **86** 021601
[173] Nitescu O, Ghinescu S and Stoica S 2020 *J. Phys.*G **47** 055112
[174] Kachelriess M, Tomas R and Valle J W F 2000 *Phys. Rev. D* **62** 023004
[175] Farzan Y 2003 *Phys. Rev.*D **67** 073015
[176] Aker M *et al* (KATRIN) 2023 *Phys. Rev.*D **107** 082005